Optimised MOPSO with the grey relationship analysis for the multi-criteria objective energy dispatch of a novel SOFC-solar hybrid CCHP residential system in the UK

Xinjie Yuan, Yuanchang Liu, Richard Bucknall

Mechanical Engineering, University College London (UCL), Gower Street, WC1E 6BT, London, UK.

Abstract

In the quest to achieve home comfort with the highest possible efficiency, there is an increasing interest in combined cooling, heating and power (CCHP) systems. These can be fuelled by natural gas and potentially by hydrogen enriched natural gas and ultimately by hydrogen. The optimised designs largely depend on the energy dispatch algorithms that take into account aspects of economic and environmental impacts as well as system efficiency. This paper details a new algorithm to optimise the operation of a novel hybrid solid oxide fuel cell (SOFC)-solar hybrid CCHP residential system. The proposed algorithm is based on the multi-objective particle swarm optimization (MOPSO) and the grey relationship analysis (GRA) (named as MOPSO-GRA) with the capability of resolving the objective energy dispatch issues within the system by effectively avoiding local optimum problem. More specifically, the grey incidences are first integrated into MOPSO to analyse the degree of closeness between non-ideal solutions and the ideal solution. Then, the relationship of degree is introduced to give

objective energy dispatch in order to maximise the efficiency of energy utilization while minimising the system capital cost, operating costs, maintenance costs, fuel costs and emissions. Finally, the new algorithm is validated on the proposed new design of CCHP system. Ten cases are studied to evaluate the technical, economic and environmental performance of the MOPSO-GRA algorithm when being applied to an SOFC-based CCHP system under both the grid-connected and the island modes. A comparison is made with the conventional MOPSO method and system structure, and the impact of a plug-in EV is also evaluated. Based on a detailed cost and emissions analysis, the results indicate the environmental and economic advantages, in addition to the higher efficiency of the proposed methodology and system structure. The impact of these results and observations leads to the promotion of intelligent FC-based multi-energy system technologies for residential use.

Keywords: CCHP, EV, Grey relationship analysis, MOPSO, SOFC.

Nomenclature

Abbreviations

AC	Absorption chiller
BT	Battery
CCHP	Combined cooling, heating and power
CH_4	Methane
CO	Carbon monoxide
CO_2	Carbon dioxide
COP	Coefficient of performance
CRF	Capital recovery factor
EV	Electric vehicle
FC	Fuel cell
FCL	Following the cooling load
FEL	Following the electrical load
FTL	Following the thermal load
GD	Grid
GRA	Grey relationship analysis
H_2	Hydrogen
H_2NG	Hydrogen enriched natural gas
H_2O	Water
HP	Heat pump
HX	Heat exchanger
LHV	Low heating value
LiBr	Lithium bromide
MILP	Mixed integer linear programming
MOPSO	Multi-objective particle swarm optimization
MPP	Maximum power point
O_2	Oxygen
PH	Pre-heating
PSO	Particle swarm optimization
PV	Photovoltaic
SC	Space cooling
SH	Space heating
SOC	State of charge
SOFC	Solid oxide fuel cell

Symbols

A_{cell}	Active area of fuel cell/heat exchanger
c_h/c_c	Specific heat capacity for hot and cold fluids
c_1/c_2	Learning factors
E_{Nernst}	Nernst voltage
$\mathrm{F}_{n_{pop,j}}$	Standardized matrix
f	Objective functions
F	Faraday's constant
g_{best}	Global best position
I	Current
i_d	Current density
k_{EV}	Index for EV charge
$\dot{n}_{1\sim9}$	Molar flow rate of species at node 1~9
$\dot{m}$	Mass flow rate
N_{cell}	Number of cells
N_{pop}	Population size of the swarm
OM	Operating and maintenance
p_{best}	Personal best position
$\dot{Q}_k$	Heat transfer rate
$Q_{BT,full}$	Battery full capacity
$r_{\mathrm{CO_2}}$	Mass of $\mathrm{CO_2}$ per 1 kg fuel consumed
r_1/r_2	Random values for MOPSO
R_j	Reference sequence
s	Number of iterations for MOPSO
U_f	Fuel utilization rate
v	Velocity of particles
V	Voltage
$\dot{x}, \dot{y}, \dot{z}$	Molar flow rate for chemical reactions

Greek symbols

η	Efficiency
γ	Grey incidence
ω	Inertia weight
ω_s/ω_e	Initial/final values of inertia weight

Subscripts/Superscripts

Act	Activation
C	Charging
Cap	Capital
Con	Concentration
D	Discharging
Eff	Efficiency
ELE	Electricity
Eva	Evaporator
Gen	Generator
Ohm	Ohmic
t	Time
tdt	Transmission, distribution and transfer

1. Introduction

Residential dwellings in the domestic sector of the UK require low-carbon electricity generation technologies and improved conservation measures to attain higher efficiencies through improved energy use [1]. Compared with industry and the transportation and the public service sector, the domestic sector witnessed the largest increase in natural gas and electricity consumption due to high heating demands [2]. The adoption of a combined cooling, heat and power (CCHP) system is an advanced technology making the most efficient use of natural resources while reducing demand on the national electricity grid, particularly during periods of maximum power consumption. Fuel cells (FCs) are especially suitable for the CCHP system because they convert chemical energy directly into electrical and thermal energy. The lower heat-to-power ratio of fuel cells compared to other power sources and prime movers leads to a greater ability to reduce the use of grid electricity and enable CO_2 reduction.

Studies pertaining to the FC-based CCHP systems are at a relatively early stage of development having emerged in 2003 with increasing interest since. Most of the research thus far has been in the area of stressing the importance of the electrochemical and thermodynamic performance of FCs in a CCHP system [3] [4] [5], rather than considering the overall operation of the FC-based CCHP system. For example, current research focuses on the impact of the mole fraction of the methane in feed gas [3], the steam-to-carbon ratio [4], the FC current density [4] and the inlet temperature of a solid oxide fuel cell (SOFC) [5] on the system electrical and thermal efficiency. The more recent advanced literature on FC-based CCHP systems can be presented by

categorizing them into four levels covering four mainstream research trends from the supply and the demand sides as shown in Fig. 1.

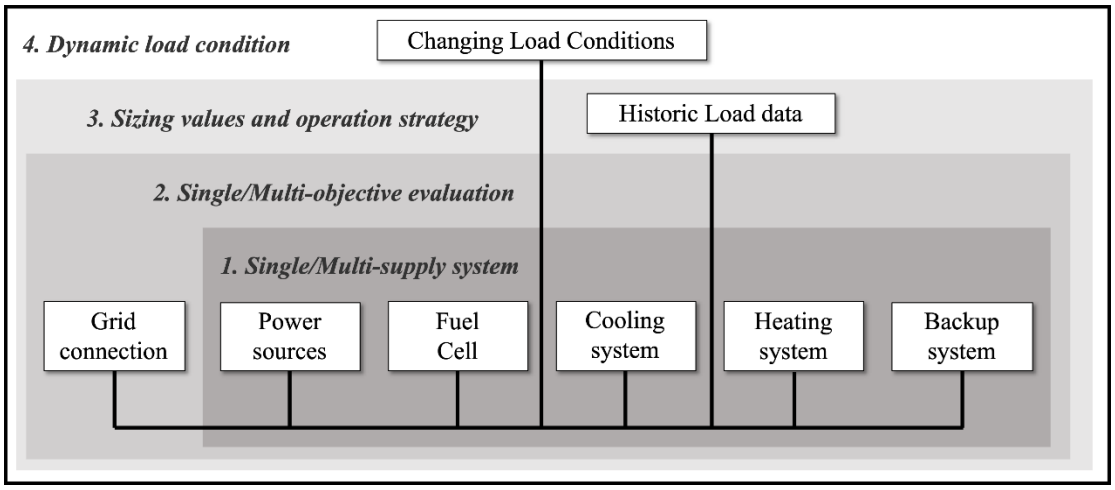

Fig. 1. Summary classification of a residential FC-based CCHP system.

1. Level 1: Among various FC-based CCHP systems, the majority of the research focuses on a single-energy CCHP system [6] [7] [8], barely considering the use of other power sources where multiple energy supplies are used. A basic FC-based CCHP system consists of a FC, with cooling, heating and backup systems. For multi-generation systems, the relationship between the electrical and thermal modelling of SOFC and other power sources is normally linearized to simplify the analysis, but this cannot reflect the accurate relationship between different fuel choices and system performance [9]. For example, solar energy is the most widely used residential renewable power source with PV panels used to provide power for electric chillers and the electrical load. This is covered in [9] for a hotel building, but the FC waste heat recovery model is insufficiently detailed. For the heating system, heat exchangers are most widely used, but the application of heat pumps is not mentioned, yet these are highly efficient devices and are compatible with CCHP systems. Some research applies

absorption refrigeration with lithium-bromide (LiBr) as the absorbent and water as the refrigerant [10] whilst others use an ammonia-water absorption chiller [11]. However, these designs regard the refrigerator/freezer as a conventional electrical device rather than a heat-driven device to make more efficient use of waste heat in a CCHP system. The demand of conventional electric freezers can be innovatively designed to be fulfilled by heat exchangers and absorption chillers to further increase the efficiency of heat use in an SOFC-based CCHP system.

2. Level 2: More attention has been paid to the SOFC standalone system under the island mode rather than the multi-energy system under the grid-connected mode. In practice, both of these modes must be given equal importance when designing the operation of a FC-based multi-energy system. Whether the grid is connected or disconnected, the system should be able to function effectively following the same system structure while providing optimal energy dispatch. However, research has focused more on the single-objective comparative analyses based on the choices of fuel inlets [12], cities [13] and load profiles [14].

3. Level 3: Sizing problems and operation strategies are two key research interests for multi-objective problems in this field. The authors' previous work in [15] [16] detailed the sizing problems for a SOFC-based CCHP system. Operation strategies can be categorised into two types, namely rule-based and optimisation-based. Rule-based operation strategies are conventional strategies and commonly they include following the electrical load (FEL), following the thermal load (FTL), and following the cooling load (FCL) in combined cooling, heat and power systems (CCHP). [17] proposed an

energy dispatch method for a CCHP from multiple renewable energy technologies with the aim of minimising costs using mixed integer linear programming (MILP). Due to the complexity of the system, the waste heat recovery system was not modelled and the relationship between the CCHP system's heat output and that of the SOFC output was linearised. Optimisation-based operation strategies can deal with nonlinear energy dispatch problems and the genetic algorithm [18] [19] approach has been applied to search for sizing values while unit commitment optimisation was used to obtain the optimal operation strategies. [20] used a multi-objective optimiser developed by the Laboratory of Industrial Energy Systems [21] to minimise the costs and CO_2 emissions and the daily operation was optimised by a linear programming method. However, the office building demand taken as the research objective in [20] was relatively constant when compared with the complexity of a domestic household's demands. Particle optimisation methods (PSO) [22] were applied to help obtain a set of non-dominated solutions which minimised emissions and costs. However, for multi-objective FC-based CCHP problems, conventional multi-objective PSO (MOPSO) cannot optimise the Pareto frontier any further or determine the ideal solution among different criteria. The particle movement trend and the selection of the global best particle from a Pareto frontier are largely influenced by the knowledge and experience of designers, which is neither objective nor efficient for the practical energy dispatch problems of multi-generation FC-based CCHP systems.

4. Level 4: Much work has been done on improving the performance of a steady-state system based on historic load data. Relatively little research has taken the dynamic large loads into consideration in order to verify practical use of the system [23].

In summary, with the promotion of private alternative fuel vehicles in the UK [24], the optimum dynamic and objective energy dispatch for CCHP systems is essential, especially when considering the changing load conditions and the switch between the grid-connected mode and the island mode. Based on the analysis of the literature, the major contributions of this paper are summarised below:

- A novel hydrogen-enriched natural gas (H_2NG)-fed SOFC-based CCHP system is designed which utilises a heat pump, photovoltaic (PV) panels and battery storage. The system is able to increase the efficiency of fuel use further by replacing conventional electric freezers with heat exchangers and absorption chillers, which is a novel concept. (See Section 2)

- Two different operation modes are introduced to cope with disconnections from the grid and other energy sources and to make the proposed system more flexible and therefore closer to practical applications. (See Sections 2 and 3)

- The new MOPSO-GRA algorithm is developed to solve the multi-criteria energy dispatch problem objectively and avoid the impact of the local optimum. Within the algorithm, the grey system theory is introduced to select the objective and ideal solution from Pareto solutions. The degree of closeness between non-inferior solutions and the ideal solution is evaluated in this algorithm to avoid falling into

local optimal solutions in a multi-criteria problem. (See Section 4)

- A practical simulation environment is created for the dynamic load condition including the charging profile of a plug-in electric vehicle (EV). By using comparative studies, the evaluation of the technical, economic and environmental performance of the CCHP system have been provided. (See Section 6)

This paper is organized as follows. The system structure, two operation modes and modelling are presented in Section 2. In Section 3, the dispatch models for the proposed CCHP system under the two operation modes are described. Section 4 presents the combination of the MOPSO algorithm and the GRA method to rationalize the multi-objective energy dispatch problem. Section 5 gives the data and the analysis for the case study. The results and a comparative analysis are discussed in Section 6 with conclusions in Section 7.

2. System illustration and modelling

2.1. System illustration

In this study, SOFC is chosen as the fuel cell in the CCHP system design for the UK energy market due to the high flexibility in fuel requirements and high temperature of SOFC resulting in a good match with the reforming unit in terms of providing a workable temperature gradient. The proposed SOFC-based CCHP system consists of an SOFC with an internal reforming unit system, an SOFC waste heat recovery sub-system, a heat pump, a photovoltaic panel system and a battery storage system which can be used under both the grid-connected mode and the island mode, as illustrated in

Fig. 2. Switches are used to control the connections of the multiple energy sources (shown in grey boxes) and the demands (shown in green boxes) in the proposed system.

It is envisaged that the electrical demands are mainly satisfied by the SOFC system, the PV system and the battery in order to minimize dependence on the national electricity grid, particularly during the periods of maximum power consumption and the charging periods of plug-in EVs. It can be observed that both the grid-connected mode and the island mode share the same SOFC waste heat recovery system as shown in the innermost dotted (rounded) rectangle. In this study, any heating and/or cooling demands are satisfied by the waste heat recovered from the SOFC system and a heat pump when the ratio of heating-to-power demand is high.

In addition to the energy flow introduced above, the conversion process is illustrated in Fig. 2 as well. For example, the inverters for the PV, FC and battery follow the P/Q control strategy under the grid-connected mode. Under the island mode, the inverters for the PV and FC with the P/Q control strategy and the inverter for the battery follows the V/f control strategy. As the conversion process is not impacting the design of the energy management method, the Simulink models for the conversion process are described briefly in an Appendix rather than in the main body of the paper.

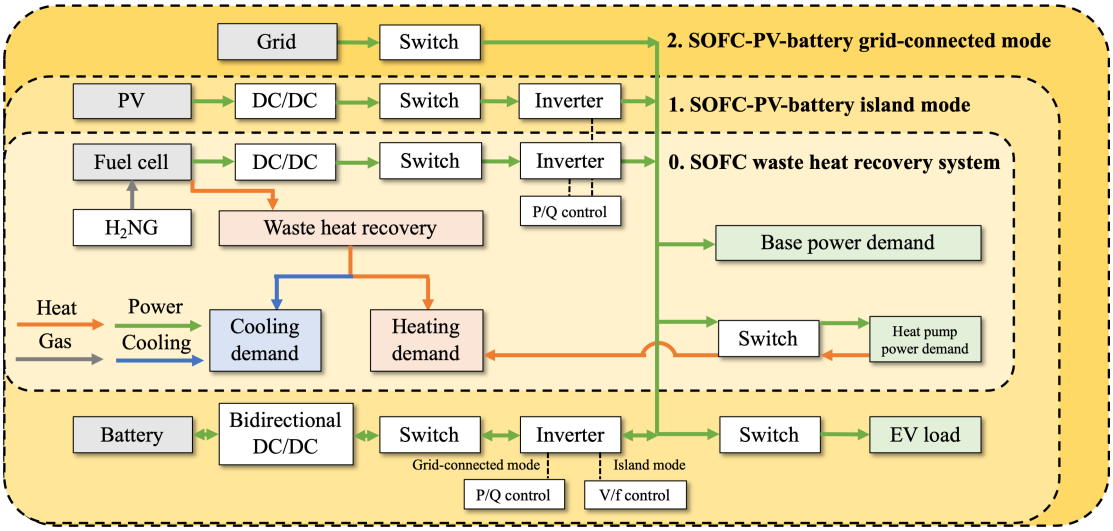

Fig. 2. Illustration of the proposed SOFC-CCHP system under two operation modes.

2.2. Assumptions

- SOFC modelling is 0-dimensional [25], where the current density in the axial direction of the tubular SOFC is an average value and is taken as being constant. The start-up of the FC is not considered.
- Fuel inlet is 20% hydrogen enriched natural gas (20% H_2NG) and all the methane is consumed in the water gas shift reaction. The excess air, unreacted hydrogen and carbon monoxide are completely combusted in the afterburner.
- Based on the authors' previous objective techniques for sizing values [15], the effectiveness of the counter-flow heat exchangers 1 through 4 are taken to be 0.6, 0.4, 0.6 and 0.7 for the air-preheating, the freezer, the domestic hot water and the space heating demands in Fig. 3. The number of SOFC cells is 71 and the operating temperature of the SOFC is 1273 K [15]. The coefficient of performance (COP) of the absorption chiller is taken to be 0.8. The COP of the heat pump is taken as 3 [26].

- Based on the energy and mass balances, the SOFC heat loss is regarded as the difference between the power output, the energy of the inputs (nodes 2 and 4) and outputs (nodes 7 and 8) in Fig. 3. Thermophysical properties of all fluids are assumed constant within the heat exchangers [27].

2.3. System modelling

2.3.1. SOFC waste heat recovery system

The SOFC waste heat recovery system is composed of an SOFC with an internal reforming system, heat exchangers, an absorption chiller and a heat pump as illustrated in Fig. 3. The hydrogen enriched natural gas (H_2NG) enters the SOFC internal reforming unit (node 1) undergoing the reforming process while part of the high-temperature exhaust stream (node 7) combined with the cathodic exhausts (node 8) passes through a catalytic after-burner (node 9). The mixture of exhaust gases first passes through heat exchanger 1 to pre-heat the air inlet (node 3). Heat exchanger 2 and absorption chiller 1 [28] are applied to satisfy the freezer demand using the heat from the exhaust gases. Domestic hot water and space heating demand are in turn delivered by heat exchangers 3 and 4. In response to the characteristics of the high heating-to-power demand ratio during the winter in the UK, a heat pump is used when needed.

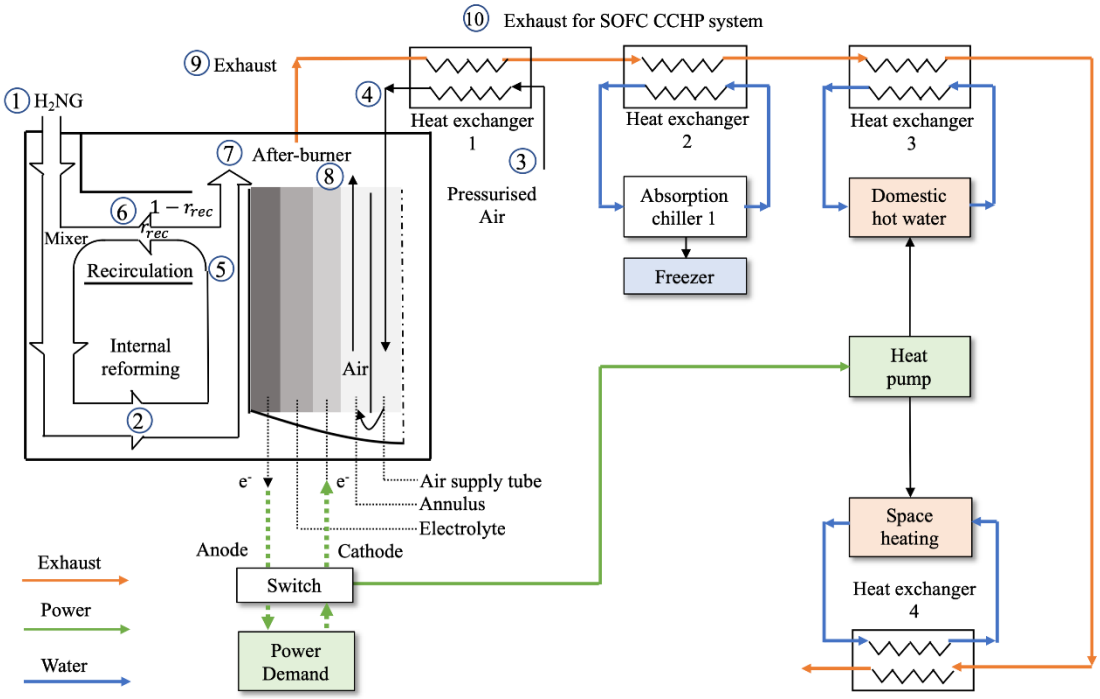

Fig. 3. Illustration of the proposed SOFC-based waste heat recovery system.

In practice, the output voltage of a FC cell V_{cell} is less than the Nernst voltage E_{Nernst} because of polarizations and other effects. These losses in voltage are a combination of electrochemical activation barriers V_{act} [29], fuel cross-over and internal current losses $V_{fuel,current}$ [30], ohmic resistance V_{ohm} [31] and concentration polarizations V_{con} [32]. These are combined in Eq. (1) [30]. The fuel cross-over and internal current losses are significant for low-temperature FCs but are neglected for devices that operate at high temperature [30]. As the main focus of the energy balance and efficiency study is the external characteristics of various system components, the detail of the internal characteristics of voltage losses and current density are not reflected in the modelling description but have been explained and validated in the authors' previous work [15].

$$V_{cell} = E_{Nernst} - V_{act} - V_{fuel,current} - V_{ohm} - V_{con} \quad (1)$$

The voltage output of a single cell can be deduced for a particular current density and operating temperature. The power output of a single cell $\dot{W}_{cell}$ [33] and a stack $\dot{W}_{FC}$ [34] can be determined by Eq. (2) and Eq. (3):

$$\dot{W}_{cell} = I \times V_{cell} = A_{cell} \times i_d \times V_{cell} \quad (2)$$

$$\dot{W}_{FC} = N_{cell} \times \dot{W}_{cell} \quad (3)$$

where I is the electrical current passed through the cell, A_{cell} is active reaction area, i_d is current density and N_{cell} is the number of cells.

At nodes 2 and 5 in Fig. 3, the steam reforming, water gas shift and electrochemical reactions of the fuel cell occur at the anodic side as below in (4) to (6) [32]:

$$\text{Steam reforming: } (\dot{x})\ (CH_4 + H_2O \rightarrow CO + 3\ H_2) \quad (4)$$

$$\text{Water gas shift reaction: } (\dot{y})\ (CO + H_2O \rightarrow CO_2 + H_2) \quad (5)$$

$$\text{Electrochemical reaction: } (\dot{z})\ (H_2 + 0.5\ O_2 \rightarrow H_2O) \quad (6)$$

where $\dot{x}$, $\dot{y}$ and $\dot{z}$ represent the mole flow rates of CH_4, CO and H_2.

Based on Faraday's law, the electrical current I passed through the cell is directly proportional to the amount of product formed [35]. The molar flow rate of hydrogen in Reaction (6) can be obtained from Eq. (7) below.

$$\dot{z} = \frac{I}{2 \times F} \quad (7)$$

where, F is the Faraday constant and $\dot{z}$ can be calculated from the assumed fuel utilization rate U_f calculated from Eq. (8).

$$U_f = \frac{\dot{z}}{\dot{n}_{2,H_2} + \dot{n}_{2,CO} + 4 \times \dot{n}_{2,CH_4}} \quad (8)$$

where the 4 in the term $4\times \dot{n}_{2,CH_4}$ is the number of hydrogen moles produced per mole of CH_4, three from the steam reforming reaction and one from the water gas shift reaction, assuming that all the methane is consumed.

The exhausts are fed to the heat exchangers as shown in Fig. 3. In this study, as the inlet conditions of hot and cold streams are known based on models above, the ε−NTU [36] approach can be applied to determine the actual heat transfer rate as only the inlet conditions of hot and cold fluids are given. For a counter-flow heat exchanger, the effectiveness (ε) can be calculated from Eq. (9).

$$\varepsilon = \frac{\dot{Q}_{actual}}{\dot{Q}_{max}} = \frac{\dot{m}_h \times c_h \times (T_{h,in} - T_{h,out})}{\min(\dot{m}_h \times c_h, \dot{m}_c \times c_c) \times (T_{h,in} - T_{c,out})} \quad (9)$$

where $\dot{Q}_{actual}$ and $\dot{Q}_{max}$ are the actual and maximum heat transfer rates, $T_{h,in}$, $T_{h,out}$, $T_{c,out}$, $\dot{m}_h$, $\dot{m}_c$, c_h and c_c are the inlet temperature, outlet temperatures, mass flow rates and specific heat capacities of hot and cold fluids respectively.

The single-effect absorption chiller, composed of a generator, a condenser, an evaporator and an absorber, is evaluated using the coefficient of performance (COP) as defined in Eq. (10) [37].

$$COP = \frac{\dot{Q}_{eva}}{\dot{Q}_{gen}} = \frac{\dot{Q}_{eva}}{\dot{m}_c c_c (T_{c,in} - T_{c,out})} \quad (10)$$

where $\dot{Q}_{gen}$ and $\dot{Q}_{eva}$ are the heat transfer rates in the generator and evaporator, and $\dot{m}_c$, c_c, $T_{c,in}$ and $T_{c,out}$ are the values obtained based on the heat exchanger model.

2.3.2. Battery system

Various types of batteries are widely used in micro grids. Lithium-ion batteries have the advantages of high energy density, fast charging, long service life and safety. In order to reflect the external characteristics of the battery system, the state of charge (SOC) is defined in Eq. (11).

$$SOC = \frac{Q_{BT}}{Q_{BT,full}} \tag{11}$$

where Q_{BT} is the energy stored in the battery and $Q_{BT,full}$ is full capacity.

2.3.3. PV system

Solar photovoltaic (PV) systems are widely used in many renewable power applications. The output characteristics model for a PV cell and a PV panel can be derived using Eq. (12) [38]. The relationship between the voltage and current is determined by the temperature and solar radiation, which is widely investigated in other research work. The details of the PV model can be obtained from [38].

$$I_{PV} = I_{ph} - I_d - I_{sh} \tag{12}$$

where I_{PV} is the PV panel output current, I_{ph} is the generated photocurrent, I_d is the direct component of t line current for a cell, I_{sh} is the current through the shunt resistor for a cell, where cells are connected in series.

In order to maximize the efficiency of a PV system, maximum power point tracking methods are normally applied to keep the power output of a PV panel near the maximum power point (MPP) for the appropriate operating temperature and solar

radiation [39]. In this study, as the data of the solar radiation and temperature are specified at hourly intervals and changes are not large, the perturbation and observation (P&O) method gives relatively good performance in keeping to the maximum power output of the PV system using Eq. (13) and (14).

$$\dot{W}_{PV} = V_{PV} * I_{PV} \tag{13}$$

$$\dot{W}_{PV\_m} = V_{PV\_m} * I_{PV\_m} \tag{14}$$

where $\dot{W}_{PV}$, V_{PV}, I_{PV} are the power, voltage and current output of the PV panel. $\dot{W}_{PV\_m}$ is the maximum power output of a PV panel when V_{PV_m} and I_{PV_m} are the voltage and current output at MPP.

3. Optimal energy dispatch

Based on the cooling, heating and power model described in Section 2, this section details the optimal multi-objective energy dispatch strategy for the grid-connected mode and the island mode, including the constraints and objective functions.

3.1. Grid-connected mode

3.1.1. Constraints

The constraints for both the grid-connected mode and the island mode consist of two parts: power, heating and cooling energy balance as shown in Fig. 4 and the upper and lower limits of the energy sources.

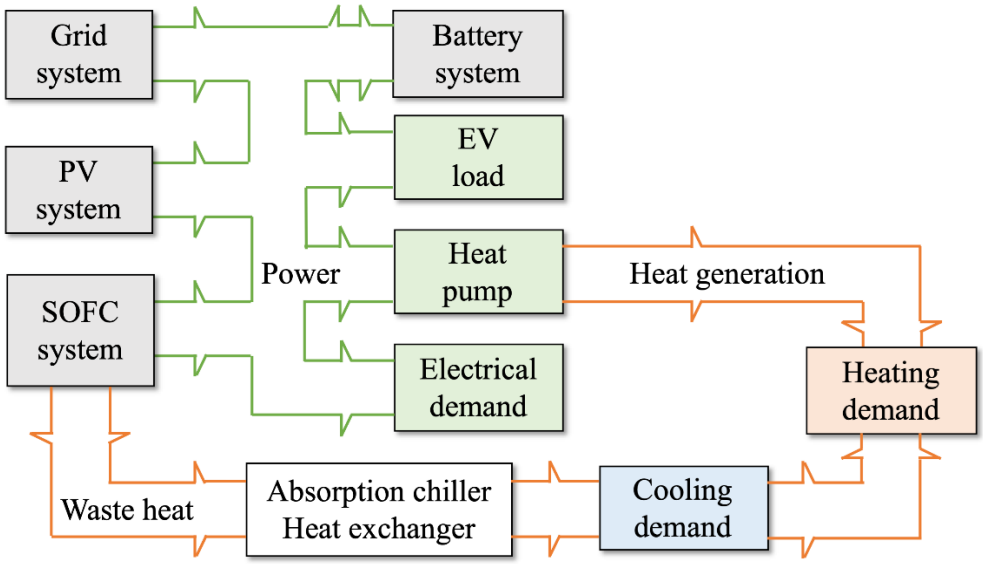

Fig. 4. System structure of the energy balance of the system under the grid-connected mode.

1) Power, heating and cooling balance:

$$\dot{Q}_{HP}^{t} = COP_{HP}\dot{W}_{HP}^{t} \tag{15}$$

$$\dot{W}_{FC}^{t} + \dot{W}_{GD}^{t} + \dot{W}_{PV}^{t} + \dot{W}_{BT}^{t} = \dot{W}_{ELE}^{t} + \dot{W}_{HP}^{t} + k_{EV} \times \dot{W}_{EV}^{t} \tag{16}$$

$$\dot{Q}_{FC}^{t} + \dot{Q}_{HP}^{t} = \dot{Q}_{PH}^{t} + \dot{Q}_{FR}^{t} + \dot{Q}_{DH}^{t} + \dot{Q}_{SH}^{t} + \dot{Q}_{SC}^{t} \tag{17}$$

where $\dot{Q}_{HP}^{t}$ and $\dot{W}_{HP}^{t}$ are the heat generated and the power consumed by the heat pump at time t, COP_{HP} is the coefficient of performance of the heat pump, $\dot{W}_{FC}^{t}$, $\dot{W}_{GD}^{t}$, $\dot{W}_{PV}^{t}$ and $\dot{W}_{BT}^{t}$ are the power provided by the SOFC system, the national grid, the PV system and the battery at time t ($\dot{W}_{BT}^{t}$ is positive when the battery is being discharged and negative when it is being charged), $\dot{W}_{ELE}^{t}$, $\dot{W}_{HP}^{t}$ and $\dot{W}_{EV}^{t}$ are the power consumed by the basic loads, the heat pump and the plug-in EV at time t, k_{EV} is the index of EV charging state (1 means the EV is being charged and 0 means not being charged), $\dot{Q}_{FC}^{t}$ and $\dot{Q}_{HP}^{t}$ are the heat provided by the SOFC waste heat recovery

system and the heat pump at time t, $\dot{Q}_{PH}^{t}$, $\dot{Q}_{FR}^{t}$, $\dot{Q}_{DH}^{t}$, $\dot{Q}_{SH}^{t}$ and $\dot{Q}_{SC}^{t}$ are the heat required for the pre-heating of the SOFC cathode inlet gases, the freezer, domestic hot water, space heating and space cooling demands at time t.

2) Power sources:

$$\dot{W}_{FC}^{min} \leq \dot{W}_{FC}^{t} \leq \dot{W}_{FC}^{max} \tag{18}$$

$$\dot{W}_{c}^{min} \leq \dot{W}_{c}^{t} \leq \dot{W}_{c}^{max} \tag{19}$$

$$\dot{W}_{d}^{min} \leq \dot{W}_{d}^{t} \leq \dot{W}_{d}^{max} \tag{20}$$

$$SOC_{min} \leq SOC^{t} \leq SOC_{max} \tag{21}$$

where $\dot{W}_{FC}^{min}$, $\dot{W}_{FC}^{max}$ are the upper and lower limit of the SOFC power outputs, $\dot{W}_{c}^{t}$ and $\dot{W}_{d}^{t}$ are the charging and discharging powers at time t, $\dot{W}_{c}^{min}$, $\dot{W}_{c}^{max}$, $\dot{W}_{d}^{min}$ and $\dot{W}_{d}^{max}$ are the maximum and minimum charging and discharging powers, SOC_{min} and SOC_{max} are the minimum and maximum state of charge (SOC) limits of the battery.

3.1.2. Objective functions

The objective functions are proposed while taking into account the two operating modes: the grid-connected mode and the island mode. For both these modes, the objectives are to maximise the integrated efficiency f_{eff}, and to minimise the cost rate f_{cost} and the emission rate $f_{emission}$.

1) The integrated efficiency f_{eff}^{t}

The efficiency of the entire system is defined in Eq. (22).

$$f_{eff}^{t} = \frac{\dot{W}_{ELE}^{t}+\dot{W}_{HP}^{t}+k_{EV}\dot{W}_{EV}^{t}+a\times\dot{Q}_{FC}^{t}}{\dot{W}_{GD}^{t}/(\eta_g\times\eta_{tdt})+\dot{m}_{H2NG,FC}^{t}\times LHV} \quad (22)$$

where $\dot{W}_{ELE}^{t}$, $\dot{W}_{HP}^{t}$ and $\dot{W}_{EV}^{t}$ are the electrical power consumed by basic loads, the heat pump and the plug-in EV at time t, $\dot{W}_{GD}^{t}$ is the electrical power imported from the grid, η_g is the power grid generation efficiency, η_{tdt} is the transmission, distribution and transform efficiency, a is the conversion rate between the electrical power and the heat energy [40], $\dot{Q}_{FC}^{t}$ is the heat that can be recovered for the freezer, domestic hot water, space heating and cooling demands at time t, $\dot{m}_{H2NG,FC}^{t}$ is the combined mass flow rate of fuel inlet for the grid and the SOFC system at time t, LHV is lower heating value of the fuel, and t denotes the time slots of the chosen day.

2) The system cost f_{cost}^{t}

When compared with the conventional systems supplied by the grid, the proposed CCHP system requires extra equipment to operate the system. Therefore, this section takes the cost of the operation of the system as one of the main objective functions. The system cost rate f_{cost}^{t} $(pence/h)$ at time t consists of three main costs: the capital cost rate for the system components f_{cap}^{t}, the operation and maintenance cost rate for the system components f_{om}^{t}, the fuel cost rate for the SOFC system f_{fuel}^{t}, and the electricity cost rate from the grid f_{ELE}^{t}.

$$f_{cost}^{t} = f_{cap}^{t} + f_{om}^{t} + f_{fuel}^{t} + f_{ele}^{t} \quad (23)$$

$$f_{cap}^{t} = \frac{CRF\times(f_{FC}+f_{PV}+f_{BT}+f_{HP}+n_{HX}*f_{HX}+f_{AC})}{N} \quad (24)$$

$$f_{om}^{t} = \sum_{p=1}^{3}(OM_p\dot{W}_p^{t}) + OM_{BT}\left[k\dot{W}_c^{t} - (1-k)\dot{W}_d^{t}\right] + \sum_{q=1}^{2}(OM_q\dot{Q}_q^{t}) \quad (25)$$

$$f_{fuel}^{t} = price_{H2NG}^{t} \times \dot{m}_{H2NG}^{t} \tag{26}$$

$$f_{ELE}^{t} = price_{GD}^{t} \times \dot{W}_{GD}^{t} \tag{27}$$

$$CRF = \frac{i_r(1+i_r)^n}{(1+i_r)^n-1} \tag{28}$$

where CRF is the capital recovery factor, f_{FC}, f_{PV}, f_{BT}, f_{HP}, f_{HX} and f_{AC} are the capital cost of the SOFC, the PV, the battery, the heat pump, the heat exchanger and the absorption chiller detailed in (29) to (34) below, n_{HX} is the number of heat exchangers which is four in this study, p is the number of components including the PV, the SOFC and heat pump, OM_p, OM_{BT} and OM_q are the operating and maintenance costs of components, $price_{H2NG}^{t}$ is the price of hydrogen-enriched natural gas, $price_{GD}^{t}$ is the price of electricity imported from the grid, $\dot{W}_{GD}^{t}$ is the electrical power imported from the grid, i_r is the interest rate (assumed as 0.5% derived from the UK's past ten-year bank rates [41]), n is the system life (20 years) [42], and N is the number of operating hours per year (8760 h/year). The expressions for the capital costs of the key system components are listed below [42], [17], [43], [44] and [45].

$$f_{FC} = 0.77 \times A_{cell} \times N_{cell} \times (2.96 \times T_{cell} - 1907) \tag{29}$$

$$f_{PV} = CAP_{PV} \times \dot{W}_{PV,max} \tag{30}$$

$$f_{BT} = CAP_{BT} \times \dot{W}_{BT,max} \tag{31}$$

$$f_{HP} = 0.77 \times 543.76(\frac{\dot{W}_{HP}}{1000})^{0.8003} \tag{32}$$

$$f_{HX} = 0.77(8500 + 409 \times (A_{HX})^{0.85}) \tag{33}$$

$$f_{AC} = 0.77[540 \times \left(\frac{\dot{Q}_{AC}}{1000}\right)^{0.872}] \quad (34)$$

where A_{cell} is the area of a single cell of the SOFC, N_{cell} is the number of cells of the SOFC, T_{cell} is the operating temperature of the SOFC, $\dot{Q}_{AC}$ is the average rate of heat extraction using the absorption chiller and A_{HX} is the total area of heat transfer of the heat exchangers.

3) The emission rate $f^t_{emission}$

The pollution damage is assessed by determining the rate of CO_2 emissions in kg/h, as below:

$$f^t_{emission} = r_{CO_2,FC} \times \dot{m}^t_{H2NG} + r_{CO_2,GD} \times \dot{W}^t_{GD} \quad (35)$$

where $r_{CO_2,FC}$ and $r_{CO_2,GD}$ are mass of CO_2 emitted per 1 kg SOFC fuel inlet and per unit of power from the grid at time t.

3.2. Island mode

3.2.1. Constraints

The equations for the upper and lower limits for the power sources remain the same. The energy balances are different when disconnected from the grid as shown in (36) and (37), and illustrated in Fig. 4.

$$\dot{W}^t_{FC} + \dot{W}^t_{PV} + \dot{W}^t_{BT} = \dot{W}^t_{ELE} + \dot{W}^t_{HP} + t_{EV} \times \dot{W}^t_{EV} \quad (36)$$

$$\dot{Q}^t_{FC} + \dot{Q}^t_{HP} = \dot{Q}^t_{PH} + \dot{Q}^t_{FR} + \dot{Q}^t_{DH} + \dot{Q}^t_{SH} + \dot{Q}^t_{SC} \quad (37)$$

3.2.2. Objective functions

The objective functions remain as for the three types as listed in Section 3.1.2. However, without the connection of the grid, the equations for efficiency, system cost and the emissions are different as below.

$$f_{eff}^{t} = \frac{\dot{W}_{ELE}^{t} + \dot{W}_{HP}^{t} + \dot{W}_{EV}^{t} + a \times \dot{Q}_{FC}^{t}}{\dot{m}_{fuel,FC}^{t} \times LHV} \tag{38}$$

$$f_{cost}^{t} = f_{cap}^{t} + f_{om}^{t} + f_{fuel}^{t} \tag{39}$$

$$f_{emission}^{t} = r_{CO_2,FC} \times \dot{m}_{H2NG}^{t} \tag{40}$$

4. MOPSO-GRA algorithm

In this section, the optimised MOPSO algorithm with grey relationship analysis is explained in detail. Generally, the aim of the optimised algorithm for the energy dispatch is to obtain an optimal and objective energy dispatch result to meet multiple criteria while avoiding the influence of human judgement.

4.1. Algorithm analysis

4.1.1. Conventional algorithms

The conventional single-objective particle swarm optimization (PSO) algorithm is a population-based stochastic optimization technique, simulating the social behaviour of bird flocking, which solves a problem with a swarm of particles, moving around within a defined search space. The movements of each particle are guided by the personal best (p_{best}) positions and the global best (g_{best}) positions of the entire population. For single-objective optimization problems, the selection of the personal best positions can

be determined by comparison with updated particle positions and there will undoubtedly be one best particle position selected as the global best position. For multi-objective energy dispatch problems, to maximise the overall system efficiency and minimise the system costs and emissions simultaneously, it is difficult to determine p_{best} through simple comparison of two particles, resulting in a Pareto set of best particles that can be selected as global best positions, none of which can be better off without causing another criterion to be worse off.

The degree of relationship $p_{n_{pop}}$ of the grey relationship analysis (GRA) quantitatively describes the interaction between factors, of which those with the same trend of development have a closer interconnection [46]. However, due to the complexity of the proposed CCHP system with its range of various variables and constraints, the conventional GRA method is unable to respond to changing load conditions.

4.1.2. New algorithm mechanism

The new MOPSO-GRA algorithm has the ability to obtain an objective set of results and to avoid falling into local optimal solutions from a set of Pareto solutions in a multi-criteria problem. The algorithm can analyse the degree of closeness between non-inferior solutions and the ideal solution. With the improved search and update process of particles and best positions, it can help designers objectively determine the operation strategy according to the three criteria discussed in Section 3.1.2 without the impact of subjectivity and inaccuracy caused by human judgement.

As illustrated in Fig. 5, the core idea of the algorithm is to guide all the particles (shown as birds) to reach the objective results based on the grey system theory (the pseudocode is provided in Algorithm 1, which is given at the end of this section). The new MOPSO-GRA algorithm is divided into three parts as shown in Fig. 5: a) Guide the search process at the s^{th} iteration; b) Update personal and global best positions at the s^{th} iteration; c) Update position and velocity of particles from the s^{th} iteration to the $(s+1)^{th}$ iteration.

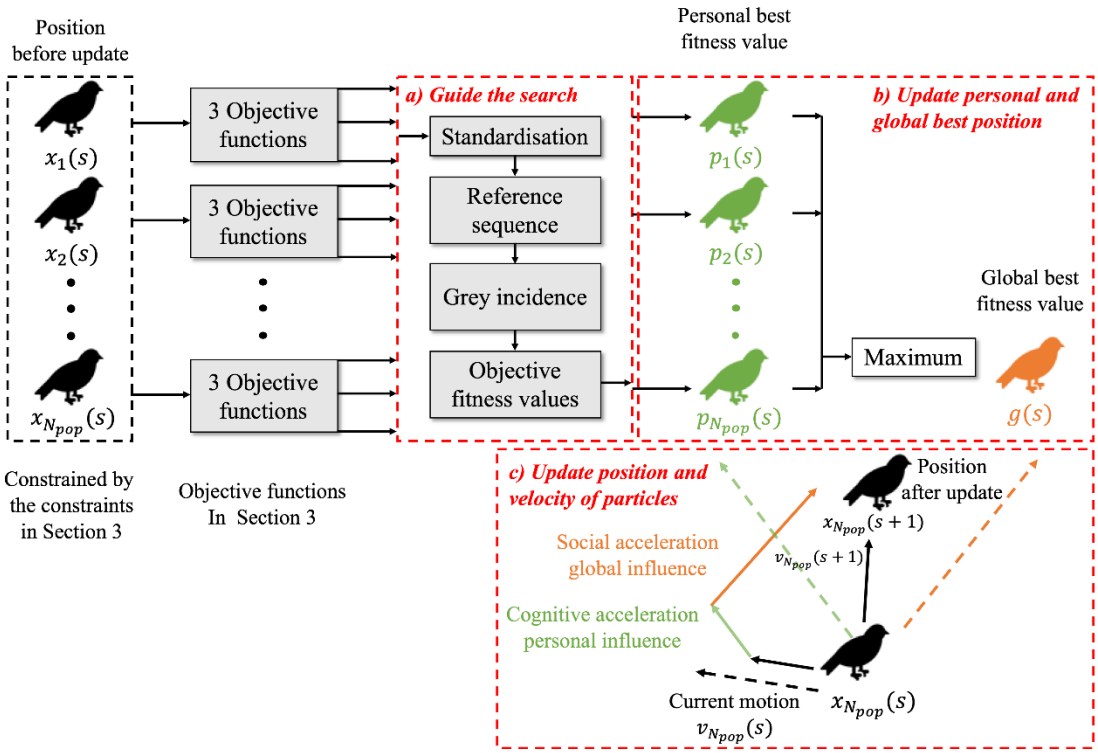

Fig. 5. Schematic diagram of the proposed MOPSO-GRA algorithm.

Initialization: The black birds in the top left corner in Fig. 5 represent the particles of a population size of N_{pop}, named a swarm at the s^{th} iteration. The swarm of particles are initialised for a matrix $(n_{supply} \times T_{hour} \times N_{pop})$, for both the position $x(s)$ and the velocity $v(s)$ of each single particle at time t at the s^{th} iteration

based on the constraints given in Eqs. (15-21) and (36-37) in Section 3.1.1 and 3.2.1. The value of n_{supply} represents the number of power sources, which is four for the grid-connected mode and three for the island mode. The value of T_{hour} is the time slots of one day, which is 24. N_{pop} is the population size of the entire swarm. These positions are evaluated by the objective functions given in Eqs. (22-35) and (38-40) in Section 3.1.2 and 3.2.2.

a) Guide the search. For the conventional MOPSO algorithm, the search process for personal and global best positions gets stuck at locally optimal values from multiple criteria. The improved algorithm introduces the grey system theory to guide the update process of particles to reach a more objective solution with an overall better performance considering multiple criteria.

The evaluation process for the guide of search includes standardisation, obtaining the reference sequence, grey incidences and objective fitness values. The three values obtained from the three objective functions for each particle.

As the three original values from the three objective functions for each particle have various dimensions and units, the matrix for all the three criteria ($N_{pop} \times 3$) at time t should be standardised [46]. For the integrated efficiency f_{eff}, the higher value is sought using Eq. (41) whilst the lower value is better for system costs f_{cost} and emissions $f_{emission}$ using Eq. (42). Therefore, for integrated efficiency, it should be standardised as follows:

$$\mathrm{F}_{n_{pop,j}} = \frac{f_{n_{pop,j}} - min_{n_{pop}=1}^{N_{pop}}(f_{n_{pop,j}})}{max_{n_{pop}=1}^{N_{pop}}(f_{n_{pop,j}}) - min_{n_{pop}=1}^{N_{pop}}(f_{n_{pop,j}})},\ j = 1 \tag{41}$$

In comparison, the standardisations of the fuel costs and emissions are expressed as follows:

$$\mathrm{F}_{n_{pop,j}} = \frac{max_{n_{pop}=1}^{N_{pop}}\left(f_{n_{pop,j}}\right) - f_{n_{pop,j}}}{max_{n_{pop}=1}^{N_{pop}}\left(f_{n_{pop,j}}\right) - min_{n_{pop}=1}^{N_{pop}}(f_{n_{pop,j}})},\ j = 2\ and\ 3 \tag{42}$$

where $\mathrm{F}_{n_{pop,j}}$ is the standardized value of the j^{th} objective function, $max_{n_{pop}=1}^{N_{pop}}\left(f_{n_{pop,j}}\right)$ and $min_{n_{pop}=1}^{N_{pop}}(f_{n_{pop,j}})$ are the maximum and minimum values from the population size N_{pop} according to each objective function at time t.

The reference sequence R_j is the maximum of each column which can be defined as:

$$R_j = \max\left[F_{1,j}, F_{2,j}, \dots, F_{n_{pop,j}}, \dots, F_{N_{pop,j}}\right] \tag{43}$$

The grey incidence $\gamma_{n_{pop,j}}$ is regarded as the proximity between the reference sequence R_j and the standardised matrix $F(n_{pop}, j)$ [46].

$$\gamma_{n_{pop,j}} = \frac{min_{n_{pop}=1}^{N_{pop}} min_{j=1}^{3}\left(F_{n_{pop,j}} - R_j\right) + \theta max_{n_{pop}=1}^{N_{pop}} max_{j=1}^{3}(F_{n_{pop,j}} - R_j)}{\left(F_{n_{pop,j}} - R_j\right) + \theta max_{n_{pop}=1}^{N_{pop}} max_{j=1}^{3}(F_{n_{pop,j}} - R_j)} \tag{44}$$

where θ is the resolution coefficient to decrease the distortion caused by the large values of $min_{n_{pop}=1}^{N_{pop}} min_{j=1}^{3}\left(F_{n_{pop,j}} - R_j\right)$. The degree of distortion is normally taken as 0.5 [46]. With the weighting coefficients and the grey incidence coefficient calculated as above, the degree of relationship $p_{n_{pop}}$ of each particle out of the entire population size can be expressed as follows [46].

$$p_{n_{pop}} = \sum_{j=1}^{3} \gamma_{n_{pop,j}} \tag{45}$$

b) Update personal and global best position. The values of the degree of relationship $p_{n_{pop}}$ of each particle are obtained as the objective fitness values, represented by the green birds as the personal best fitness values p_{best} for each particle. As a higher coefficient of the grey incidence represents a higher correlation of the particle to the three criteria, the global best fitness value g_{best} is the maximum of the personal best fitness values.

c) Update position and velocity of particles. The update of the velocity and the position of the particles at the s^{th} iteration follows the personal best fitness value and the global best fitness value. The degrees of relationship are compared with the personal best at each iteration s and further updates are made to find the personal best and global best. The positions and velocities are updated as shown below.

$$v(s+1) = \omega(s)v(s) + c_1 r_1[p_{best} - x(s)] + c_2 r_2[g_{best} - x(s)] \tag{46}$$

$$x(s+1) = x(s) + v(s+1) \tag{47}$$

$$\omega(s) = \omega_s - (\omega_s - \omega_e) \times \frac{s}{s_{max}} \tag{48}$$

where v and x are the velocity and position of particles, s is the s^{th} iteration, $\omega(s)$ is the inertia weight of particles at the s^{th} iteration, s_{max} is the maximum number of iterations, ω_s and ω_e are the initial and final values of inertia weight, c_1 and c_2 are learning factors, r_1 and r_2 are the random values between 0 and 1, p_{best} and g_{best} are the personal and global best positions.

The algorithm is detailed following the pseudocode named Algorithm 1 as below:

Algorithm 1: MOPSO-GRA algorithm

Input: Initialize population size N_{pop}, number of power sources n_{supply}, total hours T_{hour}, maximum number of iterations s_{max}, initial and final values of inertia weight ω_s and ω_e, learning factors c_1 and c_2.

for t = 1,2, … , T_{hour} **do**
- Initialize the energy dispatch matrix Z (1: n_{supply}, t, 1: N_{pop})
- **for** n_{pop} = 1,2, … , N_{pop} **do**
  - **if** matrix Z does not satisfy the constraints in Eq. (15-21) and (36-37) **then**
    - Update the matrix Z (1: n_{supply}, t, 1: N_{pop})
  - **end**
  - Evaluate the fitness functions $f_{n_{pop,j}}$ by using Eq. (22-35) and (38-40)
  - Standardize fitness functions $F_{n_{pop,j}}$ (1: n_{supply}, t, 1: N_{pop}) by using Eq. (41-42)
  - Obtain the reference sequence R_j (1, t, 1: N_{pop}) by using Eq. (43)
  - Evaluate the grey incidences $\gamma_{n_{pop,j}}$ (1, t, 1: N_{pop}) by using Eq. (44)
  - Initialize the velocity $v(s)$
  - Obtain position $x(s)$ and degree of relationship $p_{n_{pop}}$ of particles by Eq. (45)
  - Obtain the personal best position p_{best} and global best position g_{best} with the maximum degree of relationship $p_{n_{pop}}$.
- **end**
- **for** s = 1,2, … , s_{max} **do**
  - Update the inertia weight $\omega(s)$ by using Eq. (48)
  - Obtain random values for r_1 and r_2
  - Update velocity $v(s) \rightarrow v(s+1)$ by using Eq. (46)
  - Update position $x(s) \rightarrow x(s+1)$ by using Eq. (47)
  - **if** the updated positions Z does not satisfy the constraints in Eq. (15-21) and (36-37) **then**
    - Update the matrix Z (1: n_{supply}, t, 1: N_{pop})
  - **end**
  - **for** n_{pop} = 1,2, … , N_{pop} **do**
    - Evaluate fitness functions $f_{n_{pop,j}}$ by using Eq. (22-35) and (38-40)
    - Standardize $F_{n_{pop,j}}$, obtain R_j and evaluate $\gamma_{n_{pop,j}}$ and $p_{n_{pop}}$ by Eq. (41-45)
    - **if** new fitness value < fitness value $\gamma_{n_{pop,j}}$ for personal best position **then**
      - Update the personal best position and fitness value
    - **end**
    - Update the global best position and fitness value
  - **end**
- **end**

end

Output: optimal energy dispatch result

4.2. Application of the MOPSO-GRA algorithm on the SOFC CCHP system

The structural diagram of the application of the MOPSO-GRA algorithm in the novel SOFC CCHP system is illustrated in Fig. 6. As shown in Fig. 6, after satisfying the energy balances and the constraints of each component in the system, a set of the energy dispatch results for the cooling, heating and power sources is obtained. The three objective functions (technical, economic and environmental criteria) are applied to evaluate each set of the energy dispatch results.

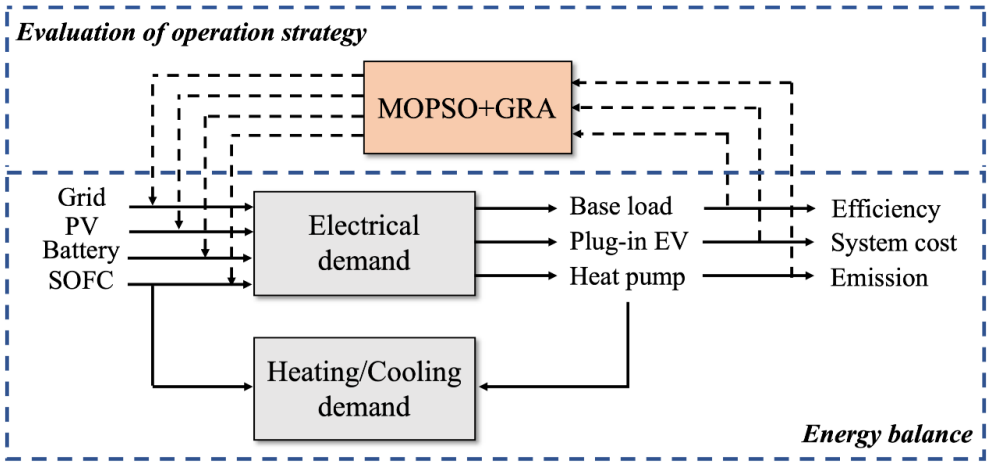

Fig. 6. Structural diagram of the application of the MOPSO-GRA methods to the operation strategy evaluation of the proposed SOFC CCHP system.

The evaluation of the energy dispatch problem, in terms of the PV, the SOFC, the battery and the national grid to basic power, heating and cooling demands, plug-in EV loads and the heat pump power demand, is determined by maximising the integrated efficiency and minimising fuel costs and emissions. Taking into account the energy balance and constraints, the optimal and objective energy dispatch result is obtained by using the MOPSO-GRA algorithm, as shown in Fig.7.

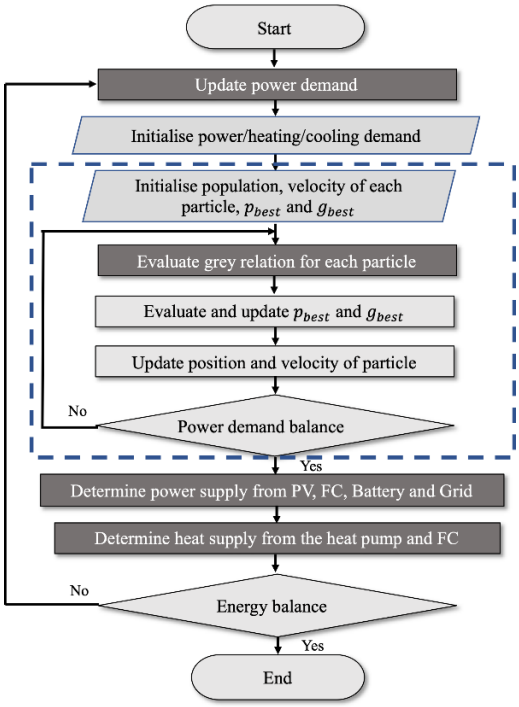

Fig. 7. The flow chart for the combination of MOPSO and GRA applied in this study.

5. Case studies

This section provides the input data for the case study of the proposed SOFC-based CCHP system using the previously described combination of MOPSO and GRA. It is based on the energy consumptions of a single non-pensioner household in the UK for the coldest day that was identified in the winter of 2010/2011 and is illustrated in Fig. 8 [47].

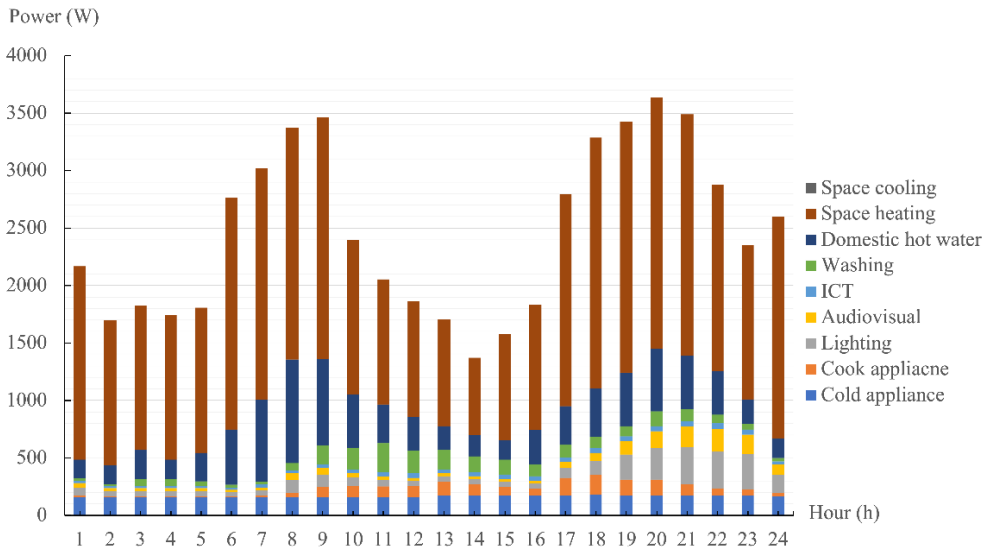

Fig. 8. Energy consumption on the coldest day in winter for a single non-pensioner household [47].

In order to test the SOFC-based CCHP with the combination of the MOPSO and the GRA method, ten cases under various system structure, operation modes, energy dispatch methods and different charging conditions of a plug-in EV are given for the analysis of the system efficiency, the system costs and the emissions. The choices of the system components used in the ten cases are summarised in Table 1.

Case 1 is a baseline without the consideration of the SOFC-based CCHP system. Cases 1-1 and 1-2 represent the conventional energy system based on the base loads (Case 1-1) and the charging profile of a plug-in EV (Case 1-2), separately. The electrical energy and freezer demands are satisfied by the power grid. The heating demands were satisfied by a boiler with an efficiency of 97% [48]. The generation efficiency η_g [49] and the transmission, distribution and transfer efficiency η_{tdt} [50] and the electricity price $price_{GD}^{t}$ [51] are given in Table 2.

Cases 2 and 3 are for the SOFC-based CCHP system in the grid-connected mode with the proposed methods and with the conventional MOPSO algorithm. Two Siemens SM55 photovoltaic modules [52] were chosen, determined by the hourly temperature [53] and solar radiation [54] in 2010 to 2011. The upper limit $\dot{W}_{FC}^{max}$ and the lower limit $\dot{W}_{FC}^{min}$ for the SOFC power output are assumed to be 800 W and 200 W. The full capacity of the battery storage system $Q_{BT,full}$ is taken as 1600 Wh and the minimum and maximum state of charge of the battery, SOC_{min} and SOC_{max}, are 0.2 and 0.8 [51]. The initial SOC value is set as 0.5. The charging and discharging powers at time t are between 0 W and 200 W. The EV selected is a 54 Chevrolet Volt with a 16 kWh battery, and it is assumed to be charged at a constant power from the SOC of 20% to 80% from 20:00 pm to 4:00 am [55]. The natural gas price, $price_{H2NG}^{t}$, [56] and [57] is given in Table 2. The values for the MOPSO method are presented in Table 3.

Cases 4 and 5 compare the performance of the proposed system operating in island mode with the two different algorithms. The impact of the plug-in EV under island mode is considered in Cases 4-2 and 5-2.

Table 1. Choices of system units and operation strategies in the ten cases.

Case	PV	FC	BT	GD	BL	HX	HP	AC	EV	Methodology
1-1/1-2				✓	✓				(✓)	Conventional
2-1/2-2	✓	✓	✓	✓		✓	✓	✓	(✓)	MOPSO+GRA
3-1/3-2	✓	✓	✓	✓		✓	✓	✓	(✓)	MOPSO
4-1/4-2	✓	✓	✓			✓	✓	✓	(✓)	MOPSO+GRA
5-1/5-2	✓	✓	✓			✓	✓	✓	(✓)	MOPSO

Table 2. Choices of system units and operation strategies in the ten cases.

	Quantity	Values
Power grid Efficiency	Generation η_g [49]	42.35%
	Transmission, distribution & transfer η_{tdt} [50]	85% to 96%
Price	Electricity from the grid $price_{GD}^{t}$ [51]	17.4 pence/kWh (0am-7am) 7.9 pence/kWh (7am-0am)
	H_2NG $price_{H_2NG}^{t}$ [56] and [57]	33.82 pence/m^3

Table 3. Key values for the MOPSO algorithm [58].

N_{pop}	ω_s	ω_e	s_{max}	c_1	c_2
300	0.9	0.4	30	2	2

The electrochemical model of the SOFC was validated in the authors' previous work [15] by comparing results with experimental data [59] and [60] for an 85% fuel utilization factor with air as the oxidant at 1273 K. The relative agreement of the cell voltage was within $\pm 7\%$, over the range for which experimental data was available [15]. Based on the energy and mass balances, the molar compositions at nodes 1 to 9 as shown in Fig. 3 are listed in Table 4.

Table 4. Chemical characteristics of gases at nodes 1 to 9 in Fig. 3 when current density is 400 mA/cm^2.

Node	Temperature (K)	Molar flux rate (mol/s)	Molar composition (%)						
			H_2	CH_4	CO	CO_2	H_2O	N_2	O_2
1	298	6.77e-5	20.06	78.35	/	/	/	1.59	/
2	1006	2.39e-4	10.62	22.20	2.66	19.22	44.40	0.90	/
3	298	3.3e-3	/	/	/	/	/	79	21
4	1055	3.3e-3	/	/	/	/	/	79	21
5	1273	3.45e-4	6.89	/	3.87	26.81	61.96	0.62	/
6	1273	1.71e-4	6.89	/	3.87	26.81	61.96	0.62	/
7	1273	1.74e-4	6.89	/	3.87	26.81	61.96	0.62	/
8	1273	3.2e-3	/	/	/	/	/	81.57	18.43
9	1353	3.3e-3	/	/	/	1.58	3.57	77.60	17.25

The capital, operating and maintenance costs of the PV, SOFC, battery, heat pump, heat exchangers and absorption chiller are listed in Table 5. The emission rate of the H_2NG fuel is 2.67 kilograms of carbon dioxide per kilogram of the fuel inlet and the carbon dioxide emission rate of the power grid is 0.2538 kg/kWh [61].

Table 5. Capital, operating and maintenance costs of components [42], [17], [43], [44], [45], [62], [63] and [64].

Component	Capital cost, CAP (£)	O&M cost, OM (pence/kWh)
FC	Eq. (29) [42]	1.5
PV	Eq. (30) [17]	0.2
BT	Eq. (31) [17]	0.1
HP	Eq. (32) [43]	0.24
HX	Eq. (33) [44]	0.08
AC	Eq. (34) [45]	0.16

6. Results and discussions

This section presents the energy dispatch results and the technical, economic and environmental analyses for the ten cases. The situation relating to the conventional system, which will be regarded as the baseline case, is outlined in Section 6.1. In Sections 6.2 and 6.3, contrasting cases present the operation strategy of the proposed system under the grid-connected mode and the island mode by using the conventional MOPSO method and the innovative combination of MOPSO and the GRA. The results are based on the loads presented in Fig. 8 and in each case they consider the connection and disconnection of the charging profile of an EV.

6.1. Conventional mode

Case 1: This conventional mode was detailed in Section 5 and the electrical power demands and the freezer demands are satisfied by electricity imported from the grid. The heating demand consists of the domestic hot water and the space heating demands and is fulfilled by a boiler with the efficiency of 97% using natural gas. The results of efficiency, system costs and emissions are taken as the reference data for the comparative analysis in Section 6.4.

6.2. Energy dispatch under the grid-connected mode

This section presents the energy dispatch results for Case 2 and Case 3, both with and without EV connection, under the grid-connected mode. The difference between Cases 2 and 3 lies in the methodology of the operation strategy.

Case 2: Fig. 9 (a) and (b) show the electrical power and heat energy dispatch results under the conventional load conditions provided in Fig. 8 while (c) and (d) consider the situation with the addition of a plug-in electric vehicle (EV). By using the combination of the MOPSO and the GRA methods, the operation strategies can be obtained at around the 13th iteration with the population size N_{pop} of 300 which is significantly earlier than the maximum s_{max} of 30, as illustrated in Fig. 10. The grey incidences for the 24 hours given in Fig. 9 (a) and (c) represent the optimal global best fitness values according to the three criteria, the average values of which are approximately 0.78. It can be observed that the majority of the power demands are satisfied by the SOFC power output, mainly because of the higher overall efficiency of the SOFC and waste

heat recovery system resulting in lower emissions than when using power generation from the grid. From the aspect of the power demands and heating demands, it is obvious that at periods 8-10 and 18-23, the power demand is relatively higher than at other periods while at periods 6-9, 18-22, the heating demand reaches its highest values. Due to the characteristics of the FC system, another key factor that affects the results is the power-to-heating demand ratio. When the ratio increases from period 8, the grid participates by providing power. At periods 1 to 5, when the power-to-heating demand ratio is low, the grid again participates by providing power because of the influence of the low electricity price, the cost breakdown of which is detailed and compared with the unit price of electricity from the grid in Fig. 11.

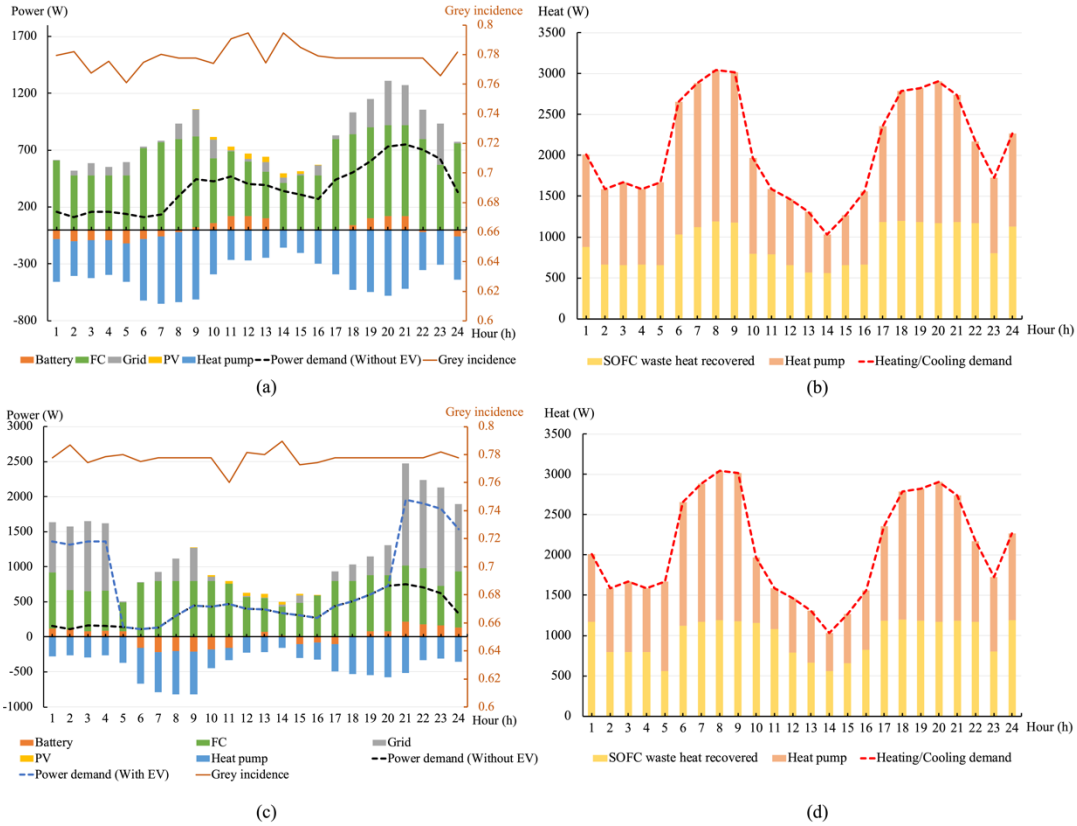

Fig. 9. Energy balances under the grid-connected mode using the combination of the MOPSO and the GRA methods: (a) and (b) are based on the base loads while (c) and (d) are based on the base loads with a plug-in EV added.

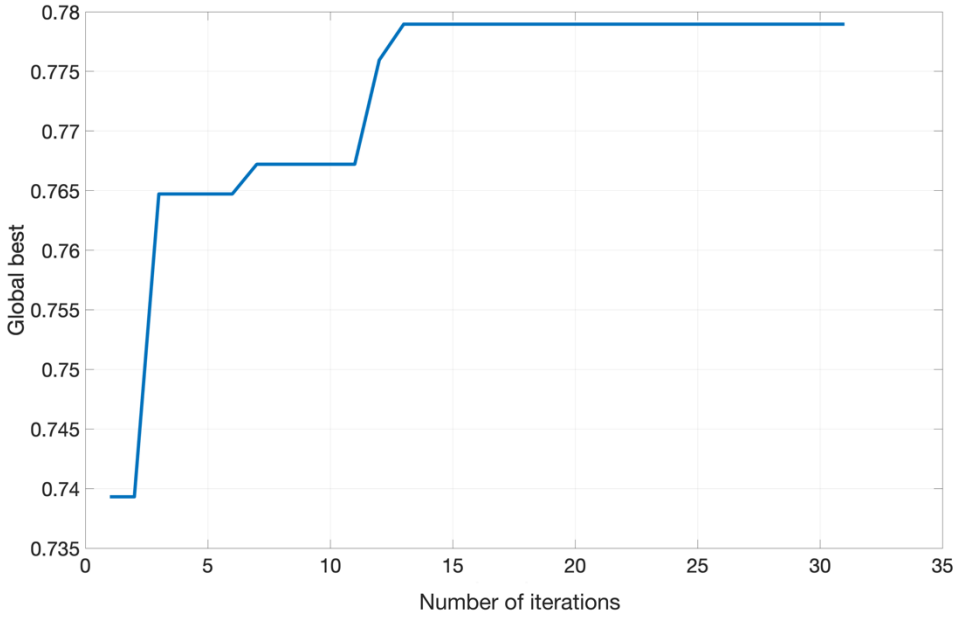

Fig. 10. The iterations of the combination of the MOPSO and the GRA methods for the global best fitness value.

The unit costs of operation of the proposed system are shown in Fig. 11 and can be divided into three main parts, the capital costsf_{cap}^{t}, the operation and the maintenance costsf_{om}^{t}, the fuel costsf_{fuel}^{t}, as described in Eq. (23). The unit cost is the three types of costs divided by the power and heating energy derived at time t. It can be seen that under the winter demands, the unit cost of the system operation is higher than the electricity price from periods 0-7, but costs less at periods 8-24. This is the reason for the participation of the grid in Fig. 9, when the power-to-heating demand ratio is low at a period of low electricity pricing.

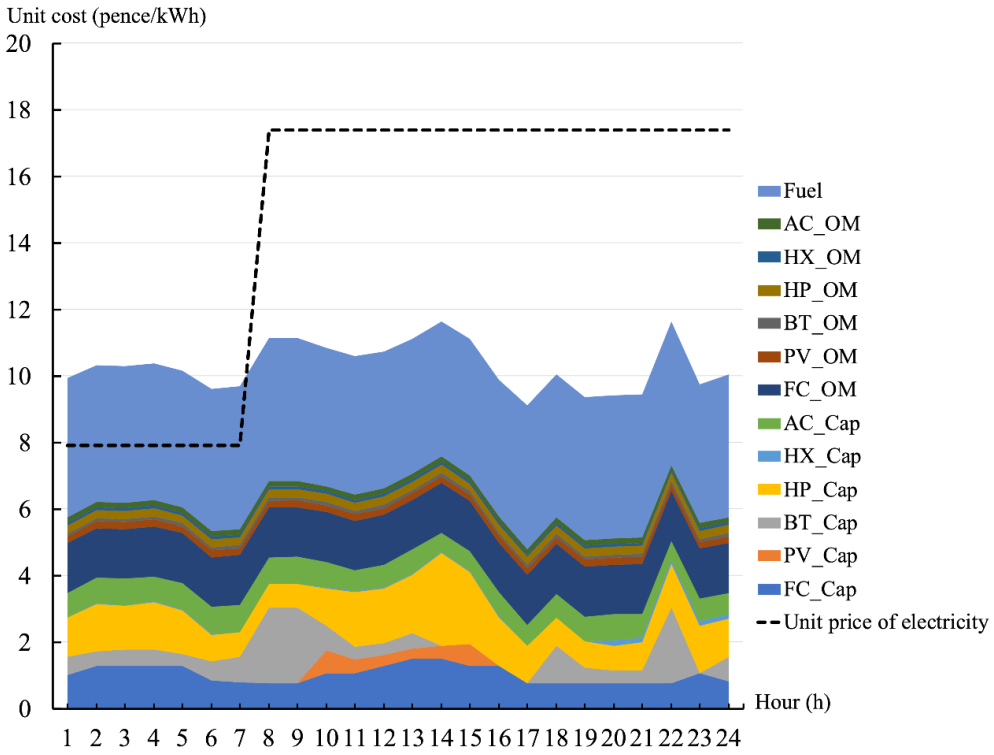

Fig. 11. Comparison of the cost breakdown of the unit costs of the proposed system with the hourly electricity price.

For the situation when the EV is charged in Fig. 9 (c) and (d), the grey incidences remain at the same level. The grid starts to provide electrical energy when the SOFC power output reaches the maximum set value during the EV charging period.

Case 3: This case is used to demonstrate the difference between the proposed algorithm and the conventional MOPSO method without the grey system method. It can be seen that the values of the grey incidences are around 0.6 in Fig. 12, about 25% lower than the values in Fig. 9, thus representing a less objective dispatch. The grey incidences are low due to the excessive participation of the grid in power provision. The demands for heat and for the freezer depend too much on the heat pump rather than the waste heat of the SOFC system. Although the operational strategies are correct

based on the constraints, the results get stalled in local optimisation and lack the consideration of the inter-connection between the various criteria.

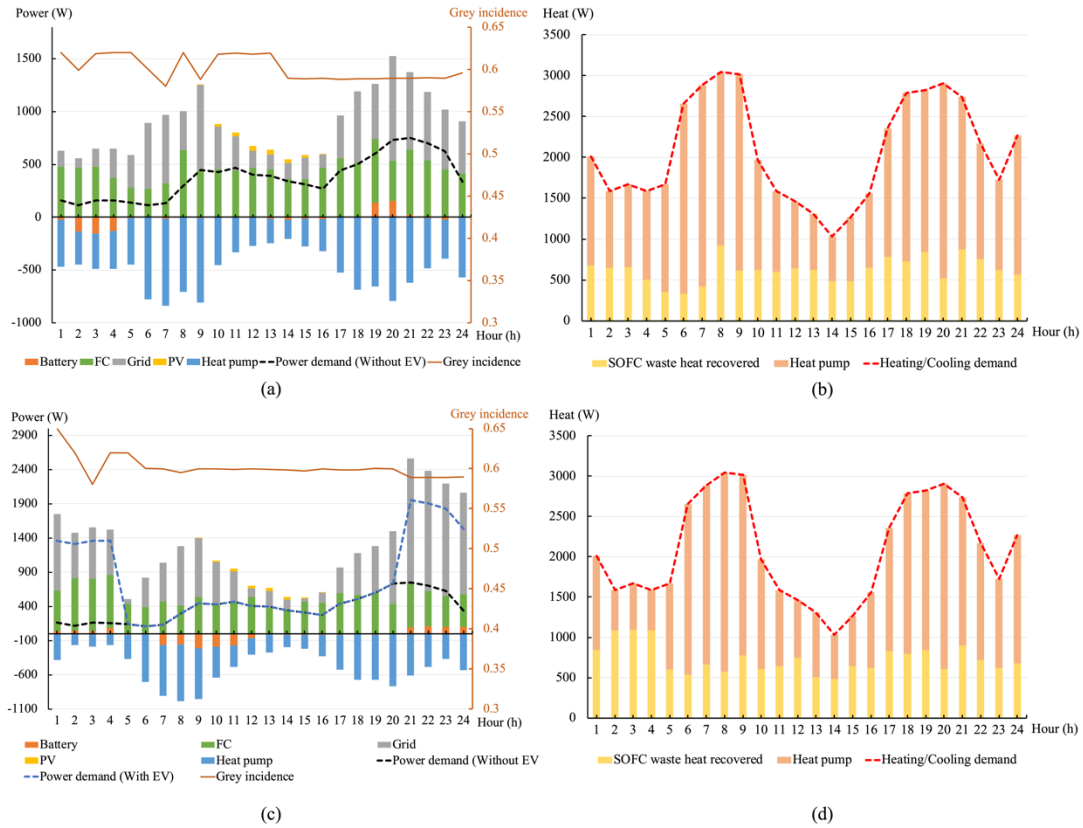

Fig. 12. Energy balances under the grid-connected mode by the conventional MOPSO method: (a) and (b) are based on the base loads while (c) and (d) are based on the base loads with a plug-in EV added.

6.3. Energy dispatch under the island mode

Cases 4 and 5: This section gives the explanation for the operation of the system under the island mode. The system is constrained by the hybrid following of the electrical load (FEL) and the following of the heating load (FHL). For example, taking (a) in Fig. 13, when the SOFC power satisfies the electrical demands but the waste heat recovered is not enough for the heating demands, the heat pump has to contribute to heat generation all the time. There is a balance between the power needed by the heat

pump, the extra power provided by the SOFC and the extra waste heat that can be recovered (as shown in Fig. 4) to maintain high efficiency of energy use. In (c), when an EV is charged during periods 21-4, the SOFC generates enough electrical energy for the EV charging and the waste heat within these hours is greater than the actual heat demand. Therefore, no energy is needed to supply the heat pump. The illustration of the energy balances with the conventional method is not displayed as it is similar to the results obtained with the proposed algorithm due to the highly coupled constraints without the compensation of the grid.

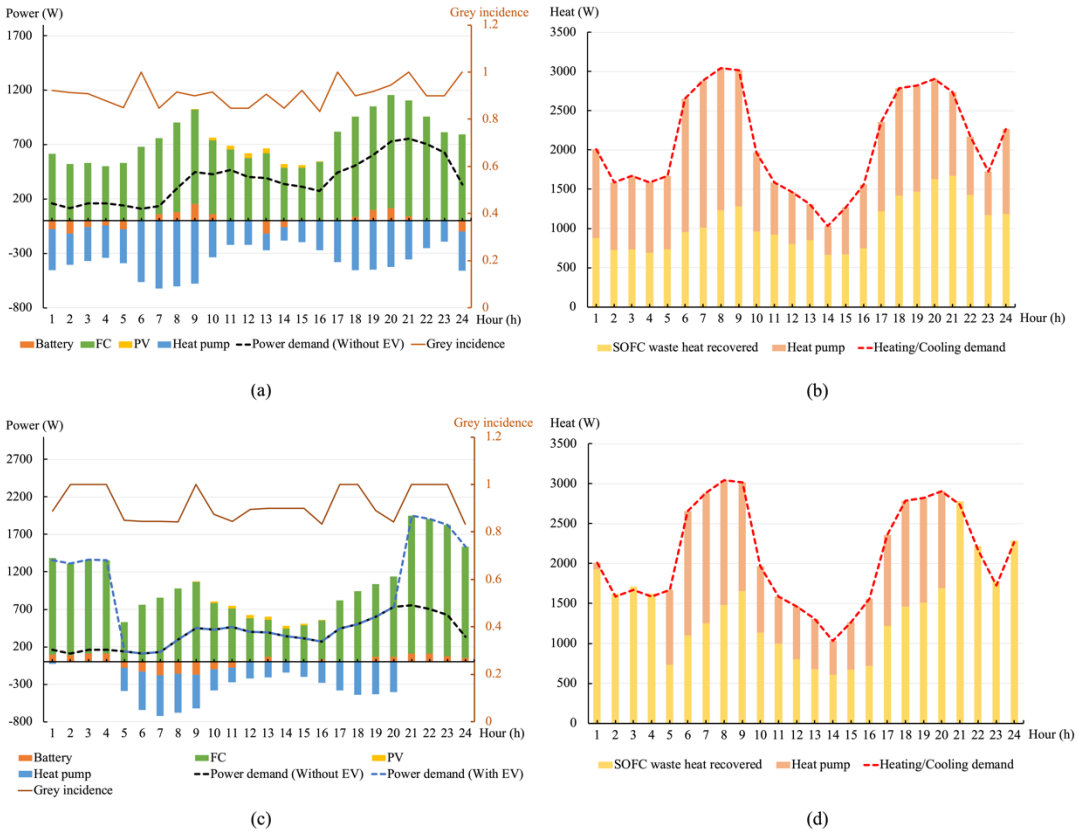

Fig. 13. Energy balances under the island mode with the combination of the MOPSO and the GRA methods: (a) and (b) are based on the base loads while (c) and (d) are based on the base loads with a plug-in EV added.

6.4. Comparative analysis

In this section, a comparative analysis is conducted to demonstrate the advantages and limitations of the proposed SOFC-based CCHP system and the novel operation strategy algorithm. The overall performances for the ten cases based on the three main criteria are summarised in Table 6 below, including the values of efficiency, the system cost rates, the emission rates and the grey incidences. These are shown for the conventional (Case 1), the grid-connected mode (Cases 2 and 3) and the island mode (Cases 4 and 5) along with the impact of the charging profile of a plug-in EV. In order to present the 24-hour data of all the ten cases clearly, the results shown in Table 6 are given as the average values.

Table 6. Technical, economic and environmental assessments for the ten cases (The values all are taken as the average values for 24 hours).

Case	Mode & methodology	EV	Efficiency	Cost rate (pence/h)	Emission rate (g/h)	Grey incidence
Case 1-1	Conventional	/	68.53%	11.82	415.41	/
Case 1-2	Conventional	✓	63.33%	16.88	516.93	/
Case 2-1	Grid + new	/	80.28%	7.19	196.46	0.78
Case 2-2	Grid + new	✓	69.54%	11.87	293.87	0.77
Case 3-1	Grid + old	/	65.20%	10.41	220.35	0.60
Case 3-2	Grid + old	✓	59.98%	15.27	315.92	0.61
Case 4-1	Island + new	/	90.05%	5.65	189.76	0.91
Case 4-2	Island + new	✓	86.88%	7.56	285.22	0.92
Case 5-1	Island + old	/	87.64%	5.94	196.83	0.89
Case 5-2	Island + old	✓	85.68%	7.92	292.23	0.88

The comparative analysis is divided into four parts to demonstrate 1) the combination of the new algorithm and the system structure over the conventional mode, 2) the application of the new algorithm over the conventional algorithm when applied to the

same proposed system, 3) the detailed cost breakdown and 4) the emission breakdown for all the ten cases.

1) The new algorithm offers better performance in terms of efficiency, cost rates and emission rates under the grid-connected mode (Cases 2-1 and 2-2) and the island mode (Cases 4-1 and 4-1) when compared with the conventional system mode (Cases 1-1 and 1-2). Based on the same demand profiles, without considering the plug-in EV, the novel algorithm delivers higher efficiency by 11.75% and 21.52% under the grid-connected mode and island mode. The system cost rates decrease by 39.17% and 52.20% and the emission rates drop by 52.70% and 54.32% under the grid-connected mode and island mode respectively. In addition, the higher load situation, when EV charging is taken into account, is shown in the four-dimensional radar chart in Fig. 14 and the differences from the aspect of these three criteria are significant . Under the grid-connected mode, the efficiency increases from 63.33% to 69.54% while the efficiency under the island mode increases to 86.88%. This is mainly because of the upper limit of the FC power output leading to the further participation of the grid when the EV is being charged. The high efficiency of the SOFC waste heat recovery system leads to decreases in the system costs by 29.68% and 55.21% under the grid-connected and the island modes. The variation of emission rates under these two modes remains at about the same level, namely 43.15% and 44.82%. Overall, the combination of the proposed system and the algorithm is more efficient, less expensive with less carbon emissions.

2) The application of the MOPSO and the GRA methods under the grid-connected mode (Cases 2-1 and 2-2) and the island mode (Cases 4-1 and 4-2) gives more objective

and optimal energy dispatch results than the conventional MOPSO method (Cases 3-1, 3-2, 5-1 and 5-2) applied to the same proposed CCHP system. The grey incidences are the best global fitness values obtained in the algorithm, representing the correlation between the three objective function results. Under the grid-connected mode, the grey incidences of the new algorithm are about 0.78, about 30% higher than the values with the conventional algorithm. A more objective energy dispatch result leads to a higher efficiency by 15.08% and 9.56%, a lower cost rate by 30.93% and 22.22%, and a lower emission rate by 10.84 and 6.98% with and without the EV charing profile. As discussed in Section 6.3, without the compensation of the electricity imported from the grid, the advantages of the new algorithm under the island mode are not as obvious as those under the grid-connected mode due to the constraints that limit the energy outputs from the different power sources. Therefore, this new algorithm can improve the performance of the system under both the grid-connected and the island modes, but it has more scope for improvement when the power sources are not highly coupled.

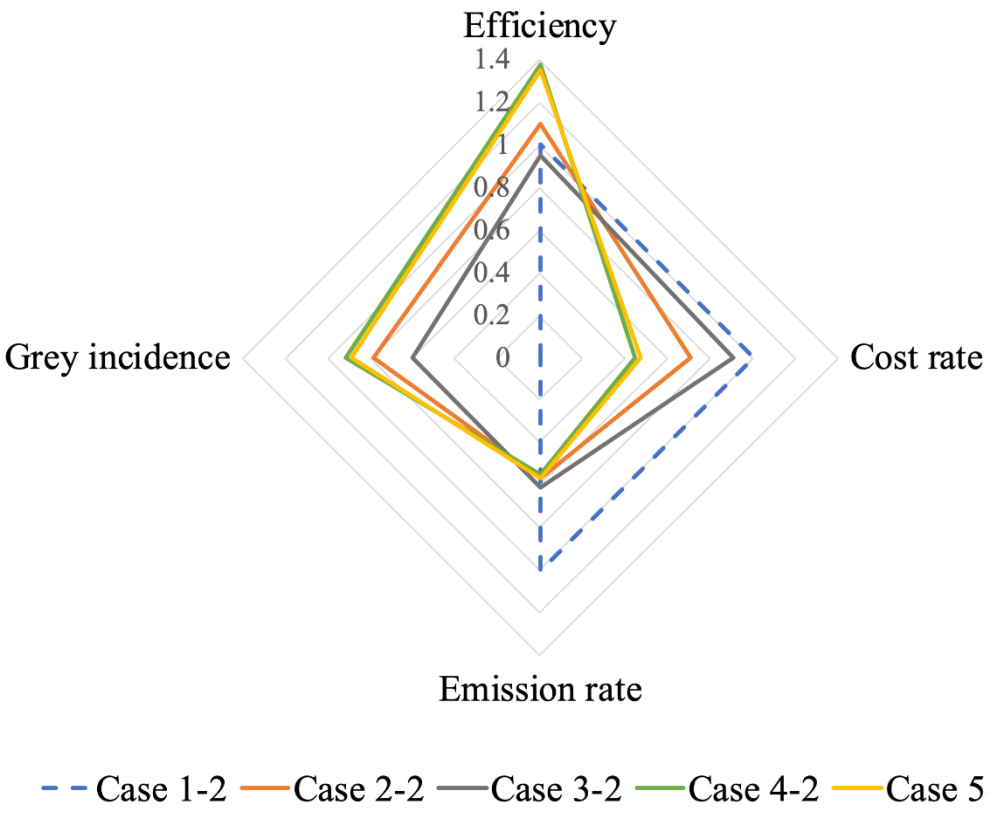

Fig. 14. Four-dimensional radar chart for the overall performance of the five cases with the EV charging profile.

3) The breakdown of the cost rates is presented in Fig. 15. The main contributions to the cost rates are the rates of the electricity cost, fuel costs, operation and maintenance costs and capital costs. It can be observed that under the grid-connected mode in Cases 2-1 to 3-2, the cost rates of importing electricity from the grid make up a relatively large percentage of the total as the price of electriciy is still higher than the H_2NG and natural gas price as illustrated in Fig. 11 in Section 6.2.

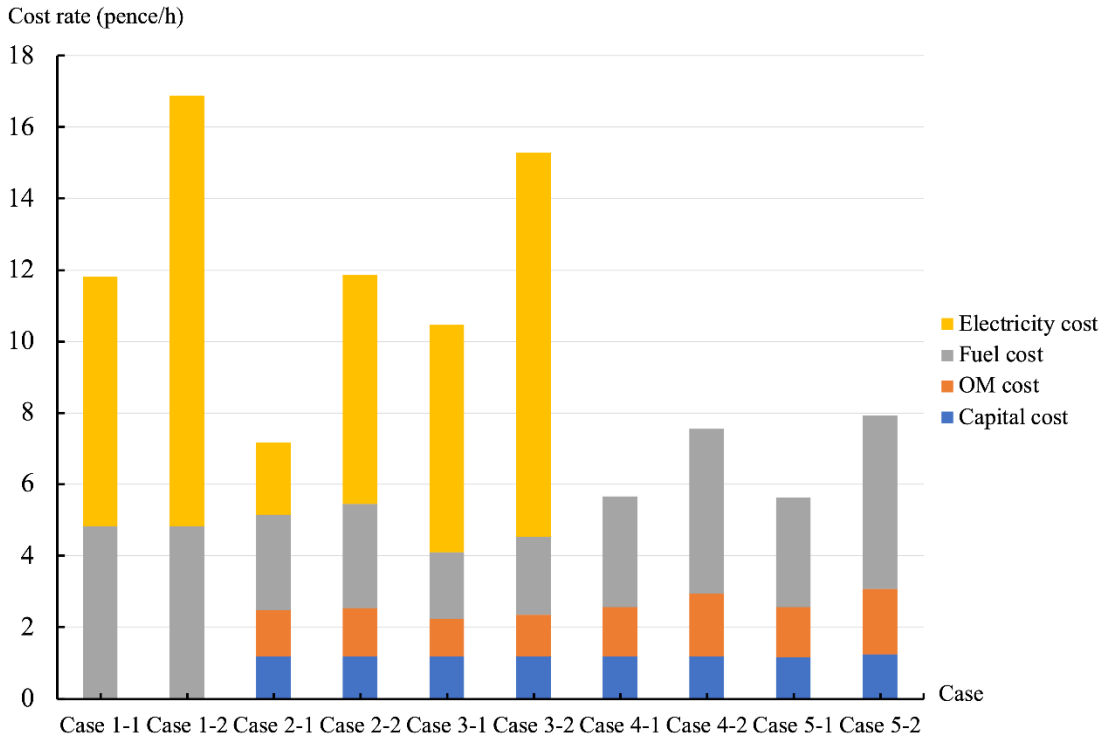

Fig. 15. Cost breakdown for the ten cases.

4) The emission analysis for the cases is illustrated in Fig. 16, consisting of the emissions from the grid and from the fuels, natural gas and H_2NG for the boiler and the SOFC system, respectively. Due to the increasing decarbonisation of the grid power generation, the differences of the carbon dioxide emissions under the grid-connected mode and the island mode are minor based on the SOFC-based CCHP system regardless of whether or not EV charging is included.

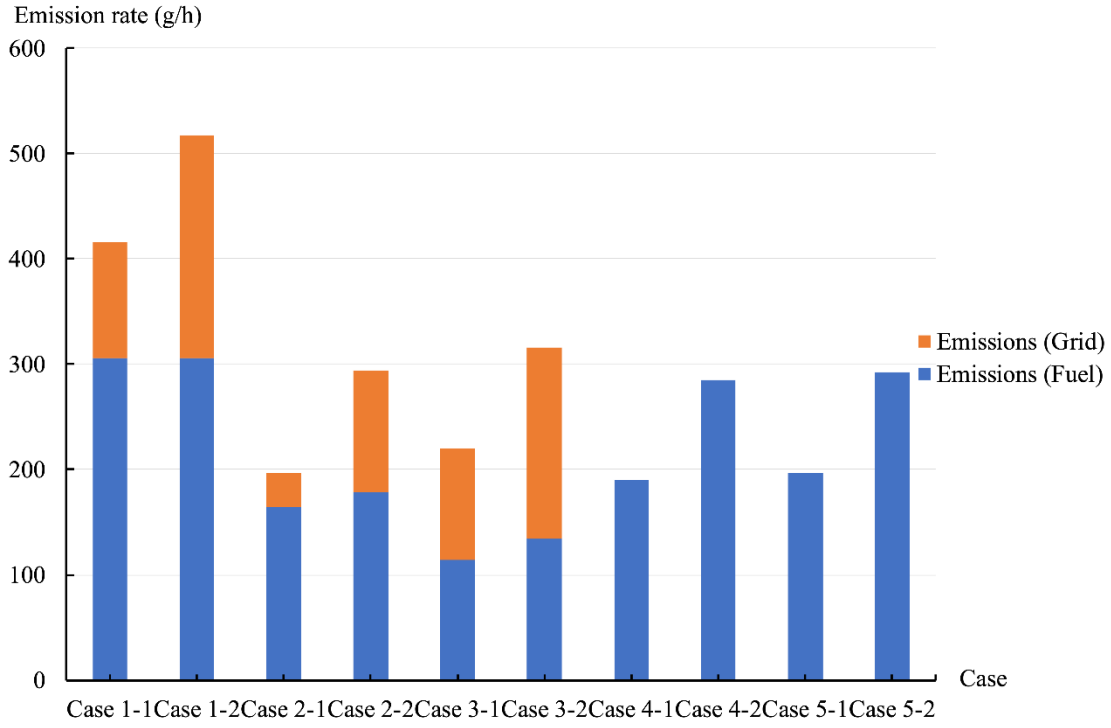

Fig. 16. Emission breakdown for the ten cases.

7. Conclusions

The significance of the work in this paper showing how to successfully integrate the grey system theory into the MOPSO algorithm for the control of a novel H_2NG-fed SOFC-based multi-generation CCHP system. Maximising the system efficiency and minimising the system costs and emissions were key design drivers. This has been achieved by introducing the concept of the grey incidence to avoid the impact of the non-objective local optimisation caused by the conventional MOPSO method when applied to a multi-criteria energy dispatch problem. The technical, economic and environmental performance of the system with the new method of control have been examined for different working modes, including the impact of charging a plug-in electric vehicle (EV). From the aspect of the system design, the freezer demand has

been innovatively regarded as heat-driven, fulfilled by the waste heat from the proposed SOFC waste heat recovery system. The model has demonstrated across ten case studies for a non-pensioner single household in the UK. The studies include a conventional system as well as the SOFC system operating in its grid-connected mode and in its island mode under the control of the novel MOPSO-GRA method and also the conventional MOPSO method. The addition of the charging profile of a plug-in EV has been also included to demonstrate the effect of a large dynamic load. The results of a detailed analysis of the cost and emissions breakdown demonstrate the combination of the system structure and the new MOPSO-GRA algorithm can improve the performance of system efficiency, system cost rates and emission rates in an objective, optimal and timely way. This work has shown the potential and the impact of the objective and intelligent SOFC-based multi-energy system technologies for residential use. The results in terms of the technical, economic and environmental criteria and the grey incidence level are summarised below:

1) Compared with the conventional system, the new combination of the proposed MOPSO-GRA method and the CCHP system increases the efficiency by between 6.2% and 23.6% whilst the rates of the system costs and the emissions are lowered by between 29.68% and 55.21% and between 43.15% and 54.32%, respectively. The degree of improvement depends on whether the system is operating in its grid-connected mode or in its island mode and whether or not EV charging is required.

2) Compared with the conventional MOPSO method, the new MOPSO-GRA method provides a higher grey incidence, increasing it from 0.60 to 0.78, which represents a

more objective energy dispatch result with closer agreement amongst the three performance criteria. Under the grid-connected mode, the new algorithm delivers a higher efficiency of between 9.6% and 15.1%, a lower system cost rate of between 22.23% and 30.93% and a lower emission rate of between 6.98% and 10.84%, depending on whether or not EV charging is considered. Even without the contribution from the power grid when operating under the island mode, the MOPSO-GRA method still provides improvement performance above that of the conventional method in terms of all the criteria, but the improvements are smaller than with the grid-connected mode. The results demonstrate that the new method performs well under both modes but is better suited to the condition when the power sources are not highly coupled and dependent on each other. Overall, the MOPSO-GRA method can assist designers and operators in determining the optimized energy dispatch strategy for a system such as the novel SOFC-based hybrid CCHP system with its multiple objectives.

Future work will address gaining revenue from the CCHP system by feeding energy into the grid at appropriate times to achieve an even lower overall system cost. A further proposal is to expand the proposed method from servicing a single household to covering a group of households with their likely different demand profiles.

Acknowledgement

The first author would like to thank China Scholarship Council (CSC) for supporting his studies at UCL. Thanks to Mr Konrad Yearwood for proof reading and valuable advice.

Reference

[1] HM Government, "Conservation of fuel and power in existing dwellings," *UK Build. Regul.*, vol. L1B, pp. 1–48, 2018.

[2] BEIS, "Energy Consumption in the UK (ECUK) 2018," *Energy Consum. UK*, no. July, pp. 1–39, 2018.

[3] B. Ghorbani, R. Shirmohammadi, M. Mehrpooya, and M. Mafi, "Applying an integrated trigeneration incorporating hybrid energy systems for natural gas liquefaction," *Energy*, vol. 149, pp. 848–864, 2018.

[4] M. Ebrahimi and E. Derakhshan, "Thermo-environ-economic evaluation of a trigeneration system based on thermoelectric generator, two-bed adsorption chiller, and polymer exchange membrane fuel cell," *Energy Convers. Manag.*, vol. 180, no. October 2018, pp. 269–280, 2019.

[5] M. Tian, Z. Yu, H. Zhao, and J. Yin, "Thermodynamic analysis of an integrated solid oxide fuel cell, Organic Rankine Cycle and absorption chiller trigeneration system with CO2 capture," *Energy Convers. Manag.*, vol. 171, no. February, pp. 350–360, 2018.

[6] Z. Yan, "Performance Analysis of the Near Zero CO2 Emissions Tri-generation System Based on Solid Oxide Fuel Cell Cycle," vol. 7, no. 10, pp. 48–50, 2017.

[7] M. Chahartaghi and B. A. Kharkeshi, "Performance analysis of a combined cooling, heating and power system with PEM fuel cell as a prime mover," *Appl. Therm. Eng.*, vol. 128, pp. 805–817, 2018.

[8] A. L. Facci, V. Cigolotti, E. Jannelli, and S. Ubertini, "Technical and economic assessment of a SOFC-based energy system for combined cooling, heating and power," *Appl. Energy*, vol. 192, no. 2017, pp. 563–574, 2017.

[9] W. Sheng *et al.*, "Stochastic multi-objective scheduling of a combined cooling, heating and power microgrid containing a fuel cell," *J. Renew. Sustain. Energy*, vol. 7, no. 6, 2015.

[10] S. Sevencan, G. Lindbergh, C. Lagergren, and P. Alvfors, "Economic feasibility study of a fuel cell-based combined cooling, heating and power system for a data centre," *Energy Build.*, vol. 111, pp. 218–223, 2016.

[11] M. Mehrpooya, H. Dehghani, and S. M. Ali Moosavian, “Optimal design of solid oxide fuel cell, ammonia-water single effect absorption cycle and Rankine steam cycle hybrid system,” *J. Power Sources*, vol. 306, pp. 107–123, 2016.

[12] G. Loreti, A. L. Facci, I. Baffo, and S. Ubertini, “Combined heat, cooling, and power systems based on half effect absorption chillers and polymer electrolyte membrane fuel cells,” *Appl. Energy*, vol. 235, no. April 2018, pp. 747–760, 2019.

[13] R. Jing, M. Wang, N. Brandon, and Y. Zhao, “Multi-criteria evaluation of solid oxide fuel cell based combined cooling heating and power (SOFC-CCHP) applications for public buildings in China,” *Energy*, vol. 141, pp. 273–289, 2017.

[14] F. Farmani, M. Parvizimosaed, H. Monsef, and A. Rahimi-Kian, “A conceptual model of a smart energy management system for a residential building equipped with CCHP system,” *Int. J. Electr. Power Energy Syst.*, vol. 95, pp. 523–536, 2018.

[15] X. Yuan, Y. Liu, and R. Bucknall, “A Novel Design of a Solid Oxide Fuel Cell-Based Combined Cooling, Heat and Power Residential System in the U.K.,” *IEEE Trans. Ind. Appl.*, vol. 57, no. 1, pp. 805–813, 2021.

[16] X. Yuan, Y. Liu, and R. Bucknall, “A novel design of solid oxide fuel cell-based combined cooling, heat and power residential system in the UK,” *8th Int. Conf. Renew. Energy Res. Appl. ICRERA 2019*, vol. 57, no. 1, pp. 212–217, 2019.

[17] Z. Li and Y. Xu, “Optimal coordinated energy dispatch of a multi-energy microgrid in grid-connected and islanded modes,” *Appl. Energy*, vol. 210, no. August 2017, pp. 974–986, 2018.

[18] B. Li, R. Roche, D. Paire, and A. Miraoui, “Sizing of a stand-alone microgrid considering electric power, cooling/heating, hydrogen loads and hydrogen storage degradation,” *Appl. Energy*, vol. 205, no. September, pp. 1244–1259, 2017.

[19] S. Soheyli, M. Mehrjoo, and M. H. Shafiei Mayam, “Modeling and optimal resources allocation of a novel tri-distributed generation system based on sustainable energy resources,” *Energy Convers. Manag.*, vol. 143, pp. 1–22, 2017.

[20] C. Weber, F. Maréchal, D. Favrat, and S. Kraines, “Optimization of an SOFC-based decentralized polygeneration system for providing energy services in an office-building in Tōkyō,” *Appl. Therm. Eng.*, vol. 26, no. 13, pp. 1409–1419, 2006.

[21] G. Leyland, “Multi-objective optimisation applied to industrial energy problems,” vol. 2572, p. 188, 2002.

[22] S. Soheyli, M. H. Shafiei Mayam, and M. Mehrjoo, “Modeling a novel CCHP system including solar and wind renewable energy resources and sizing by a CC-MOPSO algorithm,” *Appl. Energy*, vol. 184, pp. 375–395, 2016.

[23] H. Q. Nguyen and B. Shabani, “Proton exchange membrane fuel cells heat recovery opportunities for combined heating/cooling and power applications,” *Energy Convers. Manag.*, vol. 204, no. October 2019, p. 112328, 2020.

[24] Department for Transport, “Vehicle Licensing Statistics Annual 2017,” no. April, 2018.

[25] M. Karcz, “From 0D to 1D modeling of tubular solid oxide fuel cell,” *Energy Convers. Manag.*, vol. 50, no. 9, pp. 2307–2315, 2009.

[26] V. Trillat-Berdal, B. Souyri, and G. Fraisse, “Experimental study of a ground-coupled heat pump combined with thermal solar collectors,” *Energy Build.*, vol. 38, no. 12, pp. 1477–1484, 2006.

[27] S. Pradeep Narayanan and G. Venkatarathnam, “Performance of a counterflow heat exchanger with heat loss through the wall at the cold end,” *Cryogenics (Guildf).*, vol. 39, no. 1, pp. 43–52, 1999.

[28] H. T. Chua, H. K. Toh, and K. C. Ng, “Thermodynamic modeling of an ammonia-water absorption chiller,” *Int. J. Refrig.*, vol. 25, no. 7, pp. 896–906, 2002.

[29] A. Perna, M. Minutillo, E. Jannelli, V. Cigolotti, S. W. Nam, and K. J. Yoon, “Performance assessment of a hybrid SOFC/MGT cogeneration power plant fed by syngas from a biomass down-draft gasifier,” *Appl. Energy*, vol. 227, no. August 2017, pp. 80–91, 2018.

[30] G. Kaur, *Solid oxide fuel cell components: Interfacial compatibility of SOFC glass seals*. 2015.

[31] K. Zouhri and S. Y. Lee, “Tubular SOFC air electrode ohmic overpotential: Parametric and exergy study,” *Energy Convers. Manag.*, vol. 121, pp. 1–12, 2016.

[32] V. M. Janardhanan and O. Deutschmann, “Modeling of solid-oxide fuel cells,” *Zeitschrift fur Phys. Chemie*, vol. 221, no. 4, pp. 443–479, 2007.

[33] Z. Yu, J. Han, X. Cao, W. Chen, and B. Zhang, “Analysis of total energy system based on solid oxide fuel cell for combined cooling and power applications,” *Int. J. Hydrogen Energy*, vol. 35, no. 7, pp. 2703–2707, 2010.

[34] K. R. Ullah, R. K. Akikur, H. W. Ping, R. Saidur, S. A. Hajimolana, and M. A. Hussain, “An experimental investigation on a single tubular SOFC for renewable energy based cogeneration system,” *Energy Convers. Manag.*, vol. 94, pp. 139–149, 2015.

[35] J.-C. Lin, H. R. Kunz, J. M. Fenton, and S. S. Fenton, “The Fuel Cell–An Ideal Chemical Engineering Undergraduate Experiment,” *Chem. Eng. Educ.*, vol. 38, no. 1, pp. 38–47, 2004.

[36] H. A. Navarro and L. C. Cabezas-Gómez, “Effectiveness-ntu computation with a mathematical model for cross-flow heat exchangers,” *Brazilian J. Chem. Eng.*, vol. 24, no. 4, pp. 509–521, 2007.

[37] A. Lubis *et al.*, “Operation performance enhancement of single-double-effect absorption chiller,” *Appl. Energy*, vol. 219, no. January, pp. 299–311, 2018.

[38] A. Jendoubi, F. Tlili, and F. Bacha, “Sliding mode control for a grid connected PV-system using interpolation polynomial MPPT approach,” *Math. Comput. Simul.*, vol.

167, pp. 202–218, 2020.

[39] M. Mao, L. Cui, Q. Zhang, K. Guo, L. Zhou, and H. Huang, “Classification and summarization of solar photovoltaic MPPT techniques: A review based on traditional and intelligent control strategies,” *Energy Reports*, vol. 6, no. 174, pp. 1312–1327, 2020.

[40] R. Jing *et al.*, “Economic and environmental multi-optimal design and dispatch of solid oxide fuel cell based CCHP system,” *Energy Convers. Manag.*, vol. 154, no. September, pp. 365–379, 2017.

[41] A. Haldane, J. Haskel, M. Saunders, S. Tenreyro, and G. Vlieghe, “BoE Inflation Report August 2019,” no. August, 2019.

[42] L. Khani, S. M. S. Mahmoudi, A. Chitsaz, and M. A. Rosen, “Energy and exergoeconomic evaluation of a new power/cooling cogeneration system based on a solid oxide fuel cell,” *Energy*, vol. 94, pp. 64–77, 2016.

[43] G. Vialetto, M. Noro, and M. Rokni, “Innovative household systems based on solid oxide fuel cells for the Mediterranean climate,” *Int. J. Hydrogen Energy*, vol. 40, no. 41, pp. 14378–14391, 2015.

[44] H. Sadeghzadeh, M. Aliehyaei, and M. A. Rosen, “Optimization of a finned shell and tube heat exchanger using a multi-objective optimization genetic algorithm,” *Sustain.*, vol. 7, no. 9, pp. 11679–11695, 2015.

[45] H. Hajabdollahi, “Investigating the effects of load demands on selection of optimum CCHP-ORC plant,” *Appl. Therm. Eng.*, vol. 87, pp. 547–558, 2015.

[46] Y. Cenglin, “Application of Gray Relational Analysis Method in Comprehensive Evaluation on the Customer Satisfaction of Automobile 4S Enterprises,” *Phys. Procedia*, vol. 33, pp. 1184–1189, 2012.

[47] J.-P. Zimmermann *et al.*, “Household Electricity Survey: A study of domestic electrical product usage,” *Intertek*, p. 600, 2012.

[48] G. Ala, A. Orioli, and A. Di Gangi, “Energy and economic analysis of air-to-air heat pumps as an alternative to domestic gas boiler heating systems in the South of Italy,” *Energy*, vol. 173, pp. 59–74, 2019.

[49] U. Ali, C. Font-Palma, M. Akram, E. O. Agbonghae, D. B. Ingham, and M. Pourkashanian, “Comparative potential of natural gas, coal and biomass fired power plant with post - combustion CO2 capture and compression,” *Int. J. Greenh. Gas Control*, vol. 63, no. January, pp. 184–193, 2017.

[50] K. Sadovskaia, D. Bogdanov, S. Honkapuro, and C. Breyer, “Power transmission and distribution losses – A model based on available empirical data and future trends for all countries globally,” *Int. J. Electr. Power Energy Syst.*, vol. 107, no. November 2018, pp. 98–109, 2019.

[51] D. Parra, S. A. Norman, G. S. Walker, and M. Gillott, “Optimum community energy storage for renewable energy and demand load management,” *Appl. Energy*, vol. 200,

pp. 358–369, 2017.

[52] Y. Chaibi, M. Salhi, A. El-jouni, and A. Essadki, “A new method to extract the equivalent circuit parameters of a photovoltaic panel,” *Sol. Energy*, vol. 163, no. February, pp. 376–386, 2018.

[53] K. Vadodaria, D. L. Loveday, and V. Haines, “Measured winter and spring-time indoor temperatures in UK homes over the period 1969-2010: A review and synthesis,” *Energy Policy*, vol. 64, pp. 252–262, 2014.

[54] M. Perry and N. Golding, “The range of environmental temperature conditions in the United Kingdom,” no. May, p. 25, 2011.

[55] G. Pareschi, L. Küng, G. Georges, and K. Boulouchos, “Are travel surveys a good basis for EV models? Validation of simulated charging profiles against empirical data,” *Appl. Energy*, vol. 275, no. July, p. 115318, 2020.

[56] J. Cooper, L. Stamford, and A. Azapagic, “Economic viability of UK shale gas and potential impacts on the energy market up to 2030,” *Appl. Energy*, vol. 215, no. February 2018, pp. 577–590, 2018.

[57] S. De-León Almaraz, C. Azzaro-Pantel, L. Montastruc, and M. Boix, “Deployment of a hydrogen supply chain by multi-objective/multi-period optimisation at regional and national scales,” *Chem. Eng. Res. Des.*, vol. 104, pp. 11–31, 2015.

[58] J. Cai, X. Ma, Q. Li, L. Li, and H. Peng, “A multi-objective chaotic particle swarm optimization for environmental/economic dispatch,” *Energy Convers. Manag.*, vol. 50, no. 5, pp. 1318–1325, 2009.

[59] S. C. Singhal, “Advances in Tubular Solid Oxide Fuel Cell Technology,” *1996 Fuel Cell Semin.*, vol. 135, pp. 28–31, 1996.

[60] M. J. Carl, “SOFC Modeling for the Simulation of Residential Cogeneration Systems,” 2008.

[61] J. Liu, Q. Yang, Y. Zhang, W. Sun, and Y. Xu, “2019 GOVERNMENT GREENHOUSE GAS CONVERSION FACTORS FOR COMPANY REPORTING Methodology Paper for Emission Factors Final Report,” *Sustain.*, vol. 11, no. 1, 2019.

[62] R. Zeng, H. Li, R. Jiang, L. Liu, and G. Zhang, “A novel multi-objective optimization method for CCHP-GSHP coupling systems,” *Energy Build.*, vol. 112, pp. 149–158, 2016.

[63] S. X. Chen, H. B. Gooi, and M. Q. Wang, “Sizing of energy storage for microgrids,” *IEEE Trans. Smart Grid*, vol. 3, no. 1, pp. 142–151, 2012.

[64] Z. Luo, Z. Wu, Z. Li, H. Y. Cai, B. J. Li, and W. Gu, “A two-stage optimization and control for CCHP microgrid energy management,” *Appl. Therm. Eng.*, vol. 125, pp. 513–522, 2017.

Appendix (can be added if required as this is part of the response to #3 Reviewer)

Fig. 2 shows that the proposed system would include DC/AC inverters. These would apply the conventional P/Q and V/f control strategies under the grid-connected and the island modes as shown in Fig. 17 and Fig. 18. Under the grid-connected mode, the inverters follow the P/Q control strategy. Under the island mode, the PV and FC remain with the P/Q control strategy while the battery takes the V/f control strategy. As the control strategy for the inverters of the PV and SOFC remain the same under both modes, the details of these two subsystems are not repeated in Fig. 18.

The DC/DC boost circuit of the PV takes the perturbation and observation method for maximum power point tracking. The values of the reference power for the SOFC boost and the battery buck/boost circuit are obtained from the result of the proposed energy dispatch method.

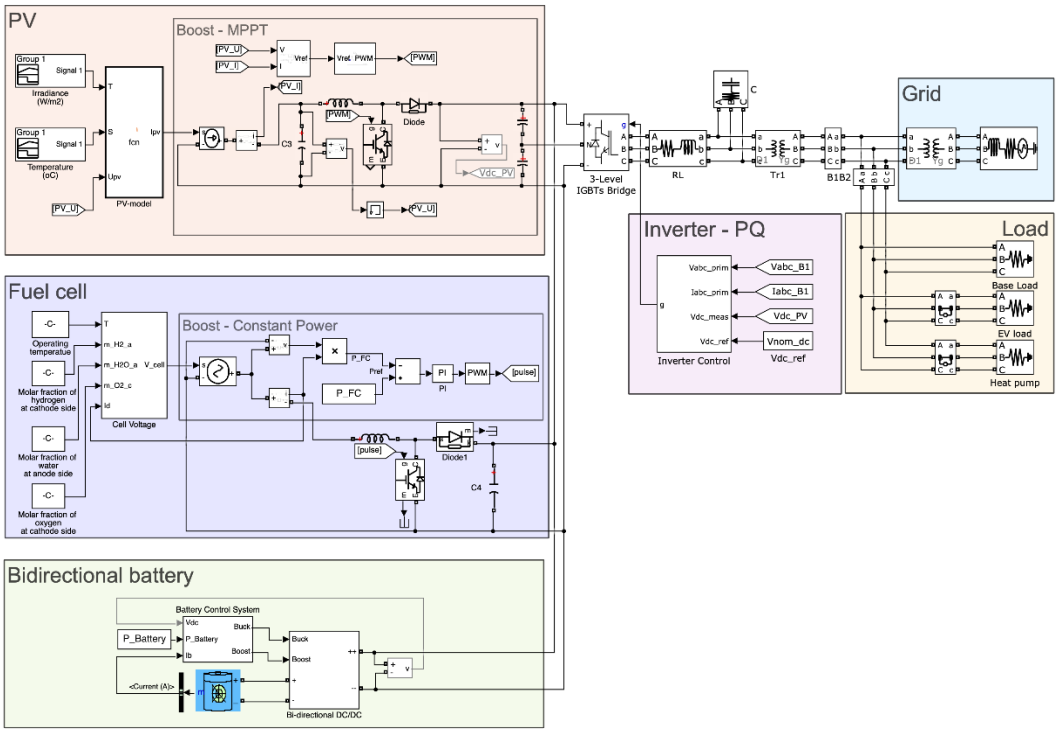

Fig. 17. The Simulink model of the proposed system under the grid-connected mode.

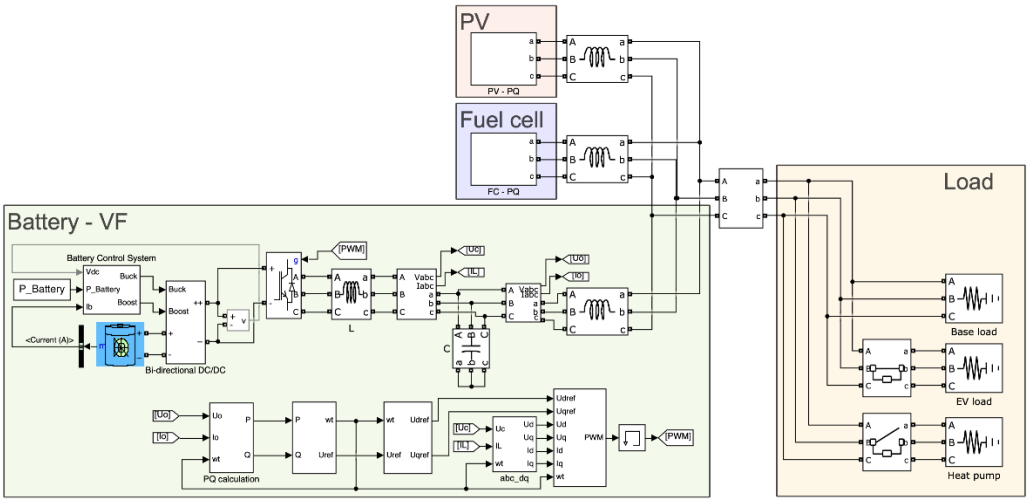

Fig. 18. The Simulink model of the proposed system under the island mode.

Part of the simulation results are given in Fig. 19 and Fig. 20 separately for the two modes. Taking the example of the energy dispatch result for the period 1 to 2 in Fig. 12 (c), the reference value of the FC power is changed from 600 W to 800 W at 0.3s as shown in Fig. 19 (a). It can be seen in Fig. 19 (b) and (c) that the voltage and current of phase a are in-phase and have good dynamic response when the environment changes.

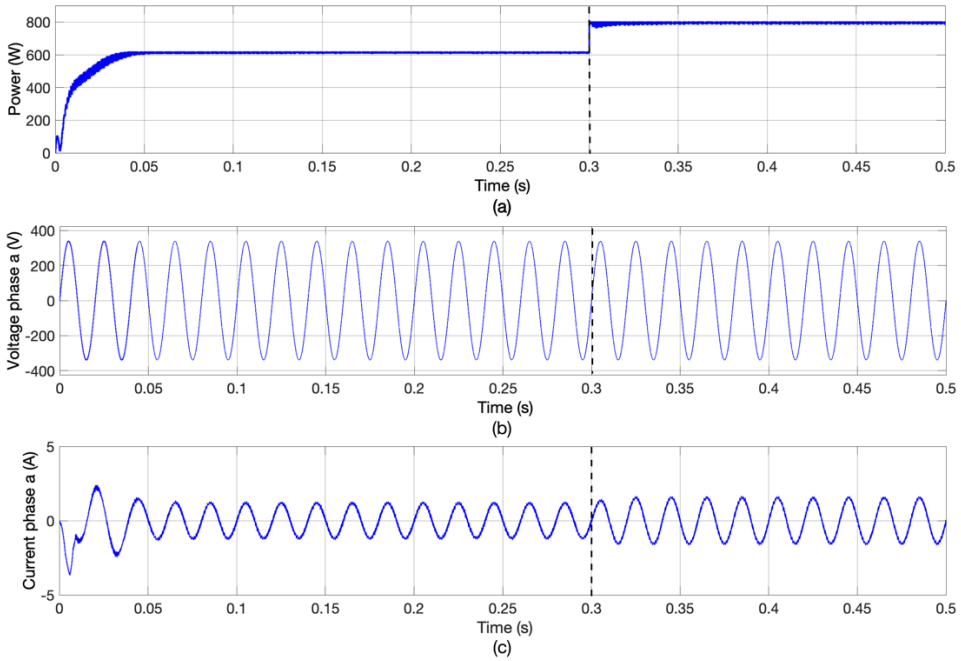

Fig. 19. The Simulink result of the system under the grid-connected mode. (a) the power output of FC; (b) the voltage of phase a; (c) the current of phase a.

Taking the example of the energy dispatch result from period 9 to 10 as shown in Fig. 13 (a), the load change is assumed to happen at 0.3s in the Simulink model as shown in Fig. 20. Fig. 20 (a) gives the power outputs of the PV, FC and battery and Fig. 20 (b) shows that the frequencies of PV and FC follow the frequency of battery (V/f control) and the variation is within a reasonable range.

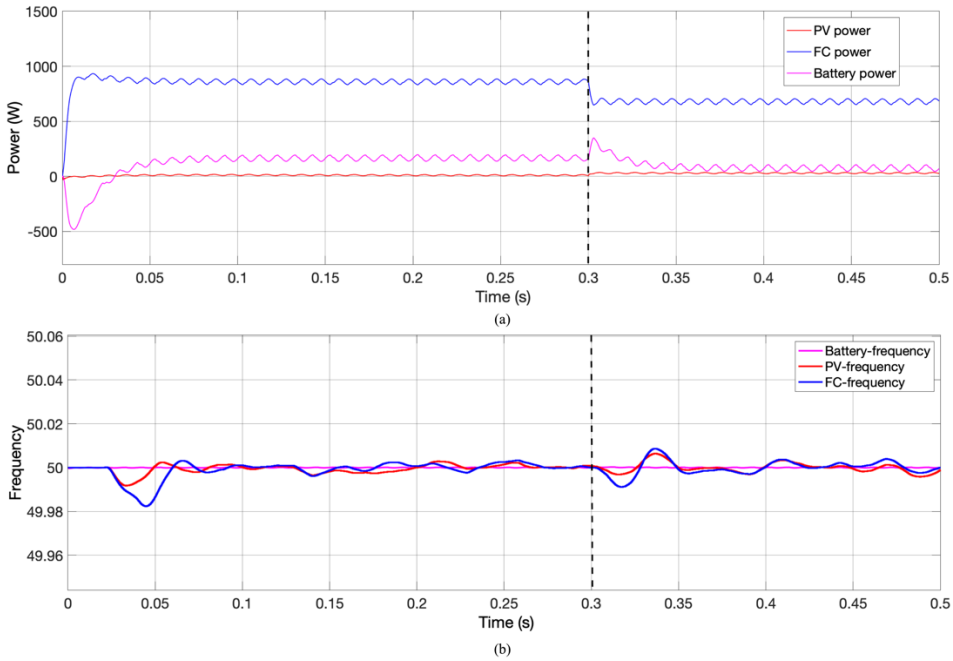

Fig. 20. The Simulink result of the proposed system under the island mode. (a) the power output of PV, FC and battery; (b) the frequency of PV, FC and battery.